AN ABSTRACT OF THE THESIS OF

Phillip J. Arscott for the degree of Master of Science in Mechanical Engineering presented on February 24, 2016.

Title: Multi Objective Aerodynamic Design in Formula SAE

Abstract approved:

_____

Robert K. Paasch

This thesis examines the effect of aerodynamics on Formula SAE cars. Due to the different objectives of the Formula SAE events, an understanding of the car's complete aerodynamic design is necessary. Using a half car computational fluid dynamics (CFD) model, a series of sensitivity studies are conducted to determine trends and interactions between each aerodynamic component and the full car. Recommendations to the car's aerodynamic design are made based on observations in sensitivity studies.

The 2013 Global Formula Racing (GFR) combustion car was then used to physically evaluate four different aerodynamic configurations and their effect to on-track vehicle performance and competition score.

# Multi Objective Aerodynamic Design in Formula SAE

by
Phillip J. Arscott

A THESIS

submitted to

Oregon State University

in partial fulfillment of
the requirements for the
degree of

Master of Science

Presented February 24, 2016
Commencement June 2016

Master of Science thesis of Phillip J. Arscott presented on February 24, 2016

APPROVED:

Major Professor, representing Mechanical Engineering

Head of the School of Mechanical, Industrial, and Manufacturing Engineering

Dean of the Graduate School

I understand that my thesis will become part of the permanent collection of Oregon State University libraries. My signature below authorizes release of my thesis to any reader upon request.

Phillip J. Arscott, Author

ACKNOWLEDGEMENTS

The author would like to thank all past, current, and future Global Formula Racing team members at Oregon State University and DHBW Ravensburg. There has never been an individual person or feature alone that makes the team successful, rather the continued commitment and passion of everyone involved to design and build a complete system capable of performing at the top level of Formula SAE competition.

The author would like to specifically thank members of the aerodynamics subteam for the help, ideas, and comradery to build four outstanding aero packages.

Lastly, the author would like to thank Dr. Robert Paasch for the opportunity and resources to research this topic.

TABLE OF CONTENTS Page

TABLE OF CONTENTS (continued) Page

# 1. INTRODUCTION

## 1.1 SAE International

SAE International (formerly Society of Automotive Engineers) hosts the largest collegiate design competition, Formula SAE (FSAE). Students from universities around the world are challenged to design, build, and race formula style cars under the same rule set. The competition tests the car's performance on track with a collection of dynamic events and the team's engineering knowledge in static events off track. The team with the most points at the end of the competition wins.

## 1.2 Global Formula Racing

Global Formula Racing (GFR) is the first and only internationally collaborative FSAE team. Founded in 2010, GFR consists of students from Oregon State University (OSU) in Corvallis, Oregon and DHBW Ravensburg in Friedrichshafen, Germany. The team builds two cars every year, one combustion and one electric. The cars share the same aerodynamics amongst other components. To date, GFR has won more FSAE competitions than any other team.

GFR's use of aerodynamics started in 2010 with an undertray designed by Jensen [2]. Data collected showed an increase in downforce and a decrease in lap time. Aerodynamic development continued in 2011 with the introduction of front and rear wings with an undertray. More recently, aerodynamic development has focused on methods to increase overall downforce and tailoring aerodynamic configurations to each FSAE event with the goal to maximize points at competition.

## 1.3 Formula SAE Events

The following Section includes a brief description of each FSAE event and available points. The role of aerodynamics is discussed.

### 1.3.1 Static Events

*Engineering Design - 150 points*
This event evaluates student's knowledge of the car and engineering principles used. Justification for use of aerodynamics components is necessary to earn points by providing simulation and physical testing results.

*Business Presentation - 75 points*
Students create and present a mock business plan to a panel of potential investors. The goal is to sell the investors on the idea of a car built for the weekend racer. A car with an aerodynamics package is expected to be more attractive to the weekend racer and a selling point for the car.

*Cost Analysis - 100 points*
40 points are awarded based on the total price of the car, as outlined in the FSAE cost tables [1]. Aerodynamic components increase the cost of the car and therefore reduce the number of points to be earned by the team. The remaining 60 points are based on the team's cost report and real case presentation.

### 1.3.2 Dynamic Events

In SAE dynamic events wheel to wheel racing is not allowed eliminating the need for overtaking, high top speed on straights, and excessive danger.

*Skidpad - 50 points*
This event is designed to test the car's steady state lateral acceleration by driving a series of left and right circles with an inside track radius of 7.625 meters [1]. Even though the average speed is about 40 kph [3], aerodynamic downforce will help to increase lateral acceleration and lower times. Because the vehicle is not power limited in this event, aerodynamic drag has minimal effects. The aerodynamic configuration should be tailored for maximum downforce. 50 points are rewarded to the fastest car, scaling down per SAE rules [1].

*Acceleration - 100 points*
This event tests the vehicles longitudinal acceleration. The course is completely straight with the car starting from a standstill and finishing 75 meters away. Aerodynamic downforce can help to increase longitudinal acceleration while the vehicle is traction limited by increasing vertical load on the tires. Low aerodynamic drag is preferred to increase longitudinal acceleration and top speed. 100 points are rewarded to the fastest car, scaling down per SAE rules [1]. Many teams take advantage of Rule T1.2.2 [1] to reduce aerodynamic drag in this event.

*Autocross - 150 points*
The Autocross event tests the car and driver in a course consisting of corners and straights with an intended average speed of 40 kph to 48 kph (although typical course have an average speed of 55kph to 65kph [3]). Rule D7.1 outlines the specific course requirements [1]. The course is an "A to B" style with the car starting from a standstill. Two drivers are given two attempts each, with the fastest time counting. Tire warmers are not permitted so the two attempts are made with cold tires. Aerodynamic downforce helps increase longitudinal and lateral acceleration and gives the driver confidence on cold tires. Aerodynamic drag reduces forward longitudinal acceleration and top speed. 150 points are rewarded to the fastest car, scaling down per SAE rules [1].

*Endurance - 300 points*
The Endurance event uses a similar track configuration to Autocross but with continuous laps. Two drivers must complete 11 km each, with a mandatory pit stop for a driver change. Similar to Autocross, aerodynamic downforce helps increase longitudinal and lateral acceleration and gives the driver confidence on cold tires. Aerodynamic drag reduces forward longitudinal acceleration and top speed. 300 points are rewarded to the fastest car, scaling down per SAE rules [1].

*Efficiency - 100 points*
The Efficiency event measures how efficiently the car uses fuel. Lap times and fuel used from the Endurance event are combined to determine an "efficiency factor." Aerodynamic downforce reduces lap times, increasing average speed and consequently fuel used. Aerodynamic drag increases lap times and fuel used. 100 points are rewarded to the car with the highest efficiency factor, scaling down per SAE rules [1].

## 1.4 Formula SAE Rules

This Section outlines FSAE rules relating to aerodynamics for the 2013 season [1]. Notably, FSAE rules are very open compared to other racing rulebooks. This freedom promotes creative solutions and allows students to pursue personal study in their specific area of interests. Each rule is presented below in italics, followed by comments explaining the impact the rule has on the aerodynamic design of the car.

*T1.2.2 Once the vehicle is approved to compete in the dynamic events, the ONLY modifications permitted to the vehicle are those listed below. They are also referred to in Part S of the Formula SAE Rules – Static Event Regulations.*
*i. Adjustment of wing angle, but not the location*

This rule permits changing the angle of wings at any time during the competition even while driving on track. Wing angle changes are allowed by an active or passive system.

*T2.1 Vehicle Configuration*
*The vehicle must be open-wheeled and open-cockpit (a formula style body) with four (4) wheels that are not in a straight line.*

*Definition of "Open Wheel" – Open Wheel vehicles must satisfy all of the following criteria:*
*1) The top 180 degrees of the wheels/tires must be unobstructed when viewed 68.6mm (2.7 inches) above the plane formed by the tops of the front and rear tires.*

*2) The wheels/tires must be unobstructed when viewed from the side.*

*3) No part of the vehicle may enter a keep-out-zone defined as a circle 68.6mm (2.7 inches) larger radially than the outside diameter of the tire with the tires steered*

*straight ahead with a 77kg (170 pound) driver seated in the normal driving position. The inner sidewall of the tire (vehicle side) is not included in this assessment.*

This rule more clearly defines what an open wheeled car is. It prohibits bodywork covering the tires.

*T6.2 Ground Clearance*
*Ground clearance must be sufficient to prevent any portion of the car, other than the tires, from touching the ground during track events. Intentional or excessive ground contact of any portion of the car other than the tires will forfeit a run or an entire dynamic event.*
*Comment: The intention of this rule is that sliding skirts or other devices that by design, fabrication or as a consequence of moving, contact the track surface are prohibited and any unintended contact with the ground which either causes damage, or in the opinion of the 'dynamic event organizers' could result in damage to the track, will result in forfeit of a run or an entire dynamic event*

This rule prohibits sliding skirts, which help generate downforce, commonly used by Formula 1 cars in the late 1970s.

*T9.2.1 In plain view, no part of any aerodynamic device, wing, under tray or splitter can be:*
*a. Further forward than 762 mm (30 inches) forward of the fronts of the front tires*
*b. No further rearward than 305 mm (12 inches) rearward of the rear of the rear tires.*
*c. No wider than the outside of the front tires or rear tires measured at the height of the hubs, whichever is wider.*

This rule regulates the size and location of wings and body work that could affect airflow around the car. There is no mention of height regulations which allows wings to be mounted as high as desired.

*T9.4 Ground Effect Devices*
*No power device may be used to move or remove air from under the vehicle except fans designed exclusively for cooling. Power ground effects are prohibited.*

This rule prohibits powered devices, such as fans, that move or remove air from under the car, creating suction, to fans that are part of the cooling system. This rule effectively bans "sucker" cars seen in the 1970s.

*T9.5.1 Egress from the vehicle within the time set in Rule T4.8 "Driver Egress," must not require any movement of the wing or wings or their mountings.*

This rule restricts wings mounted directly above drivers or around the cockpit that would interfere with driver egress.

*T9.5.2 The wing or wings must be mounted in such positions, and sturdily enough, that any accident is unlikely to deform the wings or their mountings in such a way to block the driver's egress.*

This rule limits wings mounted in positions that are potentially hazardous to the driver. An extremely high front wing could be considered dangerous because if it were to fail it may collapse onto the driver.

Figure 1 illustrates the keep out zones designated by the rules.

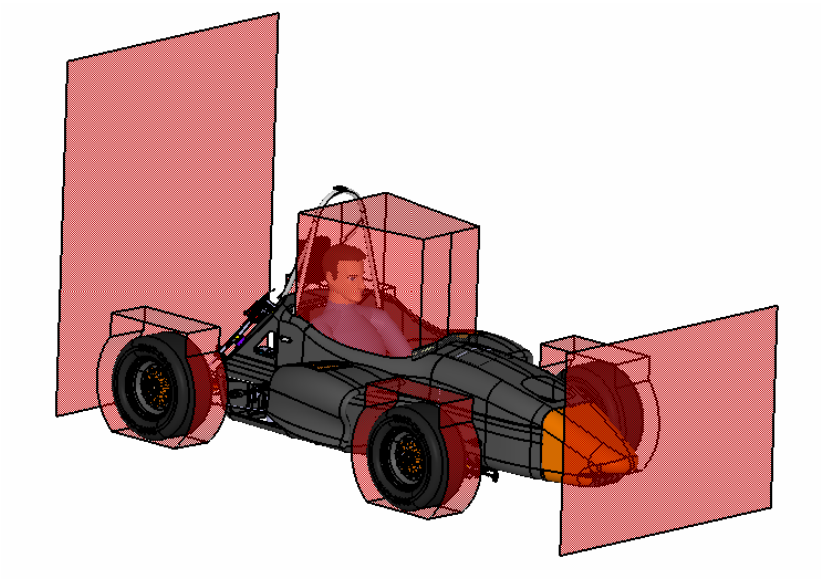

*Figure 1 Keep out zone*

## 1.5 Limiting Factors

GFR designs and builds two cars every year with the goal of competing in FSAE competitions. Therefore, all aerodynamic designs must be realistic and manufacturable with the given resources. All of the wing profiles considered in this thesis are profiles for which GFR has molds.

Other factors to consider in the aerodynamic design include the weight and reliability of the entire assembly. The wings should make enough downforce to offset their weight. Additionally, they must not fail during competition.

## 1.6 Thesis Outline

The goal of this thesis is to assist engineers designing aerodynamic components for Formula SAE. First, a literature review of aerodynamics relating to wings and wings on cars will be presented. Next, a computational fluid dynamics model will be used to conduct a series of sensitivity studies using GFR's 2013 and 2014 cars. The results of

these studies will show trends and tradeoffs between downforce and drag coefficients. Finally, four different aerodynamic configurations will be physically tested using GFR's 2013 car relating lap times and fuel used to competition score.

# 2. LITERATURE REVIEW

As presented in Section 1, the type of FSAE courses and scoring formulas reward aerodynamic downforce. The focus of this literature review is to examine existing research in low speed, high downforce aerodynamics relating to cars. In Section 4, these concepts will be applied to a full car computational fluid dynamics (CFD) simulation and interactions between different aerodynamic components will be examined.

Although the primary goal of aerodynamics in FSAE is to increase downforce, it does not come without other coupled effects. The aerodynamic design must fit with the overall car concept. The designer must identify and select designs that, as a whole, increase the car's performance. Increased drag due to higher downforce configurations must be considered, as well as added weight, complexity, and manufacturing resources involved with building the aerodynamic components. The entire system becomes highly integrated. As described in Section 1.3 the FSAE events have multiple objectives, requiring an understanding of the vehicle's complete aerodynamics.

## 2.1 Vehicle Dynamics

### 2.1.1 Acceleration

From a vehicle dynamics standpoint Wright [4] explains with Equation 1 that aerodynamic downforce is a first order performance factor to increase maximum acceleration. It is often forgotten that aerodynamic downforce will increase acceleration in all directions when the vehicle is traction limited, improving lateral and longitudinal acceleration.

$$Acceleration = Gravity \times Coefficient\ of\ friction + \frac{Downforce \times Coefficient\ of\ friction}{Mass} \quad (1)\ [4]$$

### 2.1.2 Vehicle Attitude

Yaw, pitch, and roll describe the rotational dynamics of the car. Examples of each are displayed in Figure 2. These definitions are important from an aerodynamic standpoint because they define the car's attribute with respect to the ground plane and incident air angle which can affect the aerodynamics performance of the car.

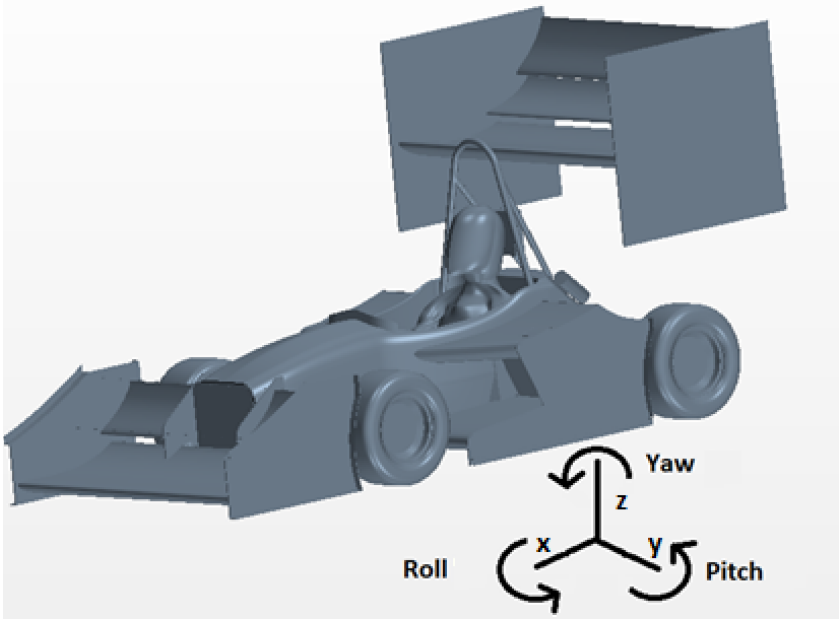


*Figure 2 Illustration of rotation directions and axes*

### 2.1.3 Aerodynamic Force Distribution

Aerodynamic force distribution, often referred to as center of pressure, is the longitudinal location of the resultant aerodynamic forces with respect to the ground plane. Katz [5] encourages the aerodynamic distribution to be located behind the car's longitudinal center of gravity to increase stability. Equations 2, 3, 4, and 5 show an example of the longitudinal aerodynamic force distribution calculation.

$$\sum My = 0 \tag{2}$$

$$\sum Fz = 0 \tag{3}$$

$$\sum Fx = 0 \tag{4}$$

$$Aerodynamic\ Force\ Distribution\ (\%rear) = \frac{Fbz}{(Fax + Fbz)} \tag{5}$$

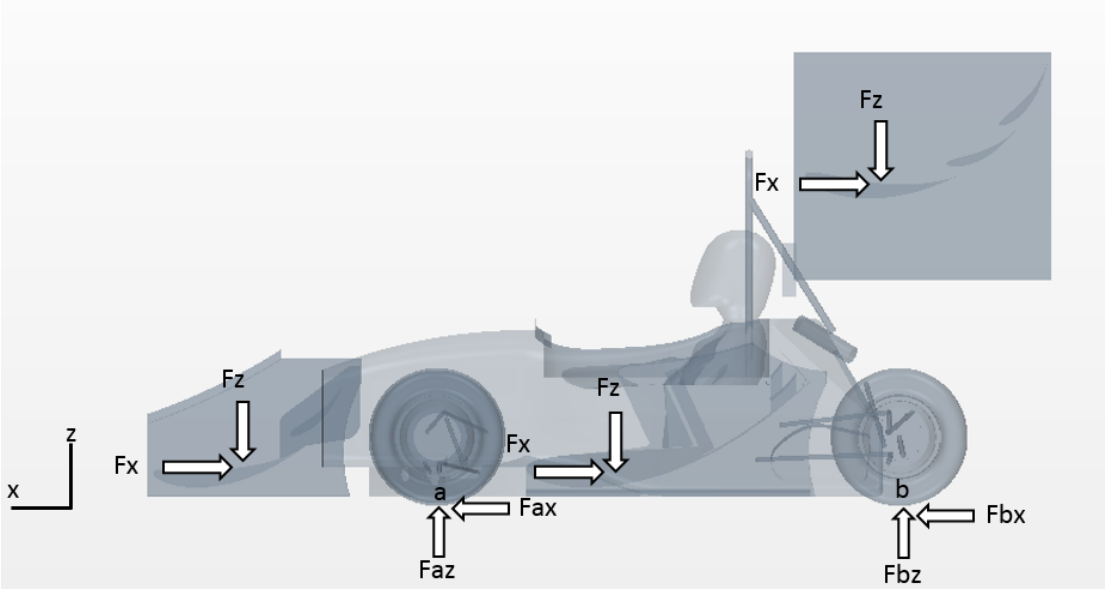


*Figure 3 Illustration of aerodynamic force distribution*

## 2.2 Aerodynamic Theory

### 2.2.1 Wing Geometry

General wing geometry is described in Figure 4. Wing span is defined as the width of the wing.

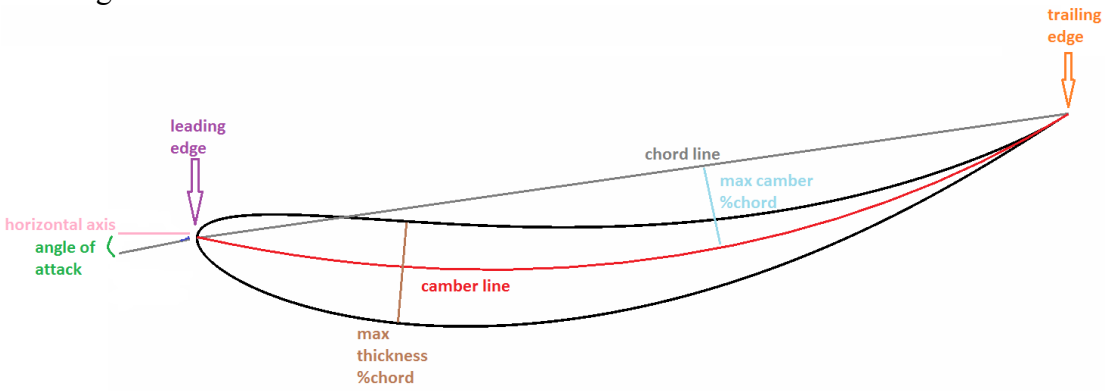


*Figure 4 Wing geometry*

### 2.2.2 Coefficient of Lift and Coefficient of Drag

Coefficient of lift (Cl), and coefficient of drag (Cd), are non-dimensional coefficients to describe and compare lift and drag of wings and cars. While not standardized, it is common to refer to a positive Cl value as a downward force in the Z direction for aerodynamics on cars. This thesis follows the same convention.

Cl and Cd for wings are defined in Equations 6 and 7.

$$Cl = \frac{2L}{\rho v^2 A_p} \tag{6}$$

$$Cd = \frac{2D}{\rho v^2 A_p} \tag{7}$$

Where:

$L = lift\ force$
$D = drag\ force$
$\rho = denisty\ of\ air$
$v = velocity\ of\ air$
$A_p = plan\ area$

Cl and Cd for cars are defined in Equations 8 and 9.

$$Cl = \frac{2L}{\rho v^2 A_f} \tag{8}$$

$$Cd = \frac{2D}{\rho v^2 A_f} \tag{9}$$

Where:

$A_f = frontal\ area$

The coefficient of lift divided by coefficient of drag is a non-dimensional coefficient to describe and compare the aerodynamics efficiency of wings and cars.

$$Efficiency = \frac{Cl}{Cd} \tag{10}$$

### 2.2.3 Angle of Attack

Angle of attack, shown in Figure 4, is the angle between a wing's chord line and the horizontal axis. It has a large influence on a wing's Cl, Cd, and Cl/Cd. Cl and Cd increase linearly with increased angle of attack until separation, normally off the trailing edge, starts to occur. A large reduction in Cl and increase in Cd is seen at even higher angles.

Different profile wings effectively change the position of this curve and maximum angle of attack before stall but have little effect on its slope [5]. Angle of attack changes are an easy way to increase Cl without additional weight. As a wing should be run close to the maximum Cl it is important to know at what angle and how abruptly Cl begins to decrease.

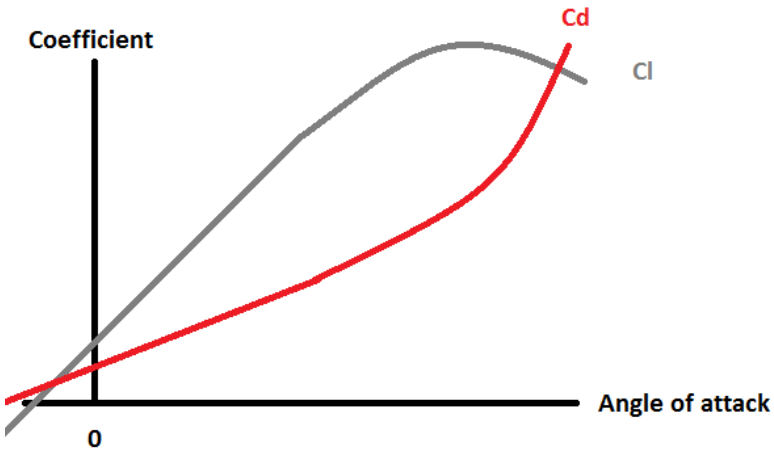


*Figure 5 Cl and Cd vs angle of attack for a generic wing*

### 2.2.4 High Lift Wing Geometry

The following Sections outlines high lift wing configurations with general design guidelines. The literature presented is more relevant to cars that operate at lower speeds and higher Cl values than aircraft.

Increasing wing span or chord has a direct impact on downforce and drag as noted in Equation (3). If higher downforce is desired, wing span and chord should be increased near the maximum allowed by the rules. The increase in wing area will increase the weight of the wing assuming the same construction is used.

Katz [5] and McBeath [6] summarize various high lift wing geometries and guidelines. Increasing a wing's camber up to 20% is possible. This allows for a higher angle of attack and higher Cl. Similarly, increasing a wing's thickness up to 20% allows for a higher angle of attack and higher Cl.

Leading edge geometry also plays a role in maximum angle of attack without separation [7]. At high angles, a more rounded leading edge is required to reduce the pressure gradient and chance of separation at the leading edge. The use of a leading edge slat is another method to prevent leading edge separation as presented in Section 2.2.7 [8].

### 2.2.5 Endplates

Endplates are vertical components fitted to the ends of wings. They effectively increase the span of the wing by reducing disturbances between the high and low pressure sides of the wing. This allows for a more consistent pressure gradient and higher Cl [6].

Research shows an increase in Cl with various endplate configurations, notably, increasing vertical height downward to have the largest effect on Cl [5], [6], [9], [10].

Wordley and Saunders [7] present wind tunnel results for a multi element wing with endplates in yaw up to 45 degrees as shown in Figure 6. Endplates account for a large stabilizing force (CS) consistent with Katz [5]. Additionally, endplate leading edge geometry (EP LE radius) was shown to help increase Cl at high yaw angles compared to a flat endplate.

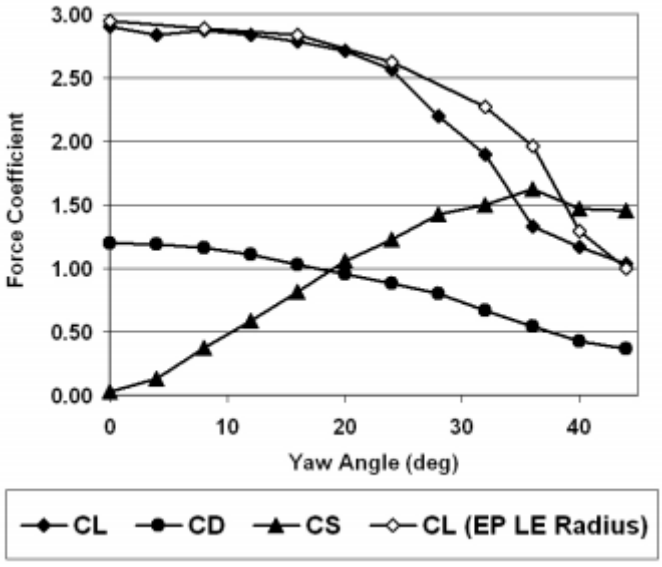


*Figure 6 Rear wing in yaw [7]*

### 2.2.6 Ground Effect

Ground effect describes wings in close proximity to the ground. The proximity to the ground helps accelerate air underneath the wing resulting in higher Cl values than freestream [5], [6], [7], [11], [12], [13], [14]. A wing's proximity to the ground is described in Equation 11.

$$ground\ proximity = \frac{h}{c} \tag{11}$$

Where:

$$h = lowest\ height\ of\ the\ wing$$
$$c = chord\ length$$

Ground effect can be seen at h/c <1 [14]. Maximum Cl occurs between h/c = 0.05 and h/c = 0.10 [7], [14], [12] and is dependent on wing geometry. Similar to wings in freestream, Cl increases at higher angle of attacks [7], [14] , [13]. The rate of Cl increase compared to angle of attack is steeper for a wing in ground effect [13]. An abrupt reduction in Cl is seen when the wing is too close to the ground caused by too steep of a pressure gradient resulting in separation [12].

Similar to angle of attack, choosing the correct h/c is an effective way to increase Cl without additional weight.

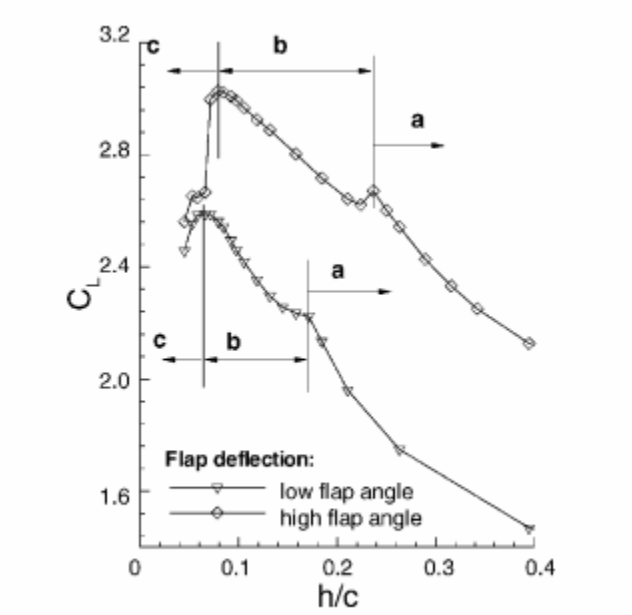


*Figure 7 Cl vs h/c for a two element wing in ground effect [14]*

Unlike other research of wings in ground effect, Wright [4] isolates the endplate, translating it downward, while keeping h/c of the wing constant. Figure 8 shows that large increases in Cl can be achieved with low endplate heights. The low endplate prevents, high pressure, free stream air from disrupting flow underneath the wing. Here, downforce is reported by a negative coefficient of lift. Designers should pay close attention to the endplate height while still abiding by FSAE Rule T6.2.

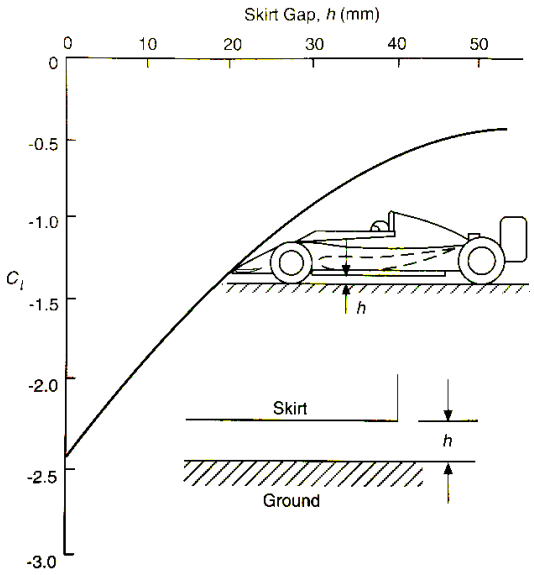


*Figure 8 Cl vs endplate height [4]*

McBeath [6] shows that the addition of a foot plate, shown in Figure 9, fitted on the lower horizontal edge of the endplate of a wing in ground effect can increase Cl by 3.4%.

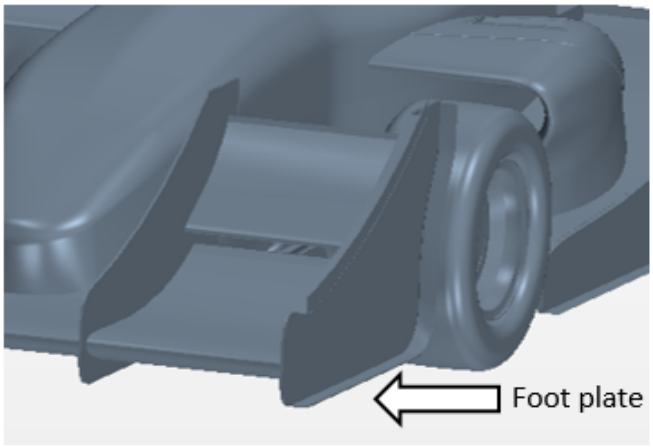


*Figure 9 Endplate foot plate*

### 2.2.7 Multiple Element Wings

Multiple (multi) element wings are wings comprised of multiple individual elements. The first large element is referred to as the "main element," with the smaller elements referred to as "flaps." Smith [8] outlines the benefits of multi element wings. These wings are able to achieve higher angles of attack without separation and consequently a higher Cl than a single element wing [5], [6], [15]. A Cl of 4 can be achieved with multi element wings [8]. Figure 10 shows geometry of a typical multi element wing.

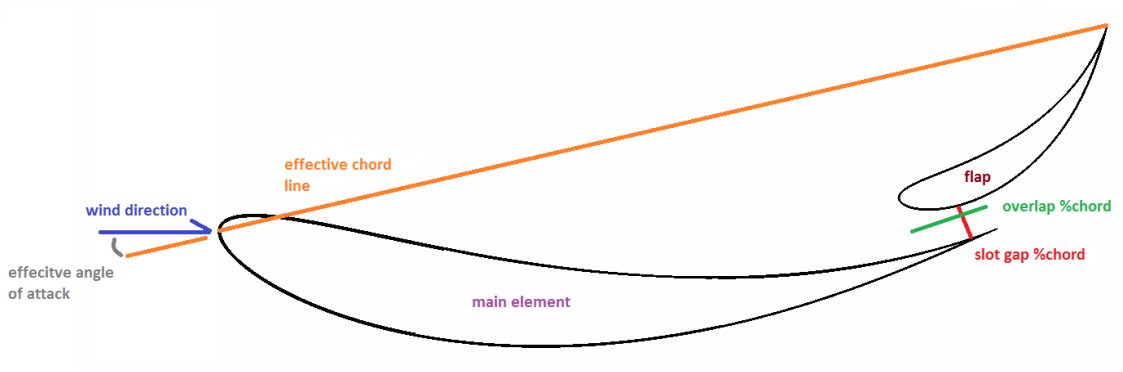


*Figure 10 Multi element wing geometry*

McBeath [6] provides guidelines for designing multi element wings. Flaps should be 25%-40% of chord length of the main element with a slot gap 1%-2% of chord length and an overlap 1%-4% of chord length.

Stacked wings, or bi-plane wings, can be used to increase Cl although interactions between elements result in lower Cl values than if the wing were in free stream. Vertical spacing of one chord length should be maintained [5]. Stacked wing configurations are common when the rules limit the allowable space for wings.

### 2.2.8 Gurney Flaps

Gurney flaps are add on devices placed at the trailing edge of the high pressure side (top) of the wing. They are used to increase Cl and decrease Cd (in some applications). Typical Gurney flap sizes range from 1%-5% of chord length. The gurney flap increases the wing's effective angle of attack and allows the wing to operate at higher angles of attack before separation occurs [16], [17], [18]. Gurney flaps can be changed or removed which makes them a quick and convenient way of fine tuning Cl, Cd, Cl/Cd, or center of pressure. Additionally, Gurney flaps placed vertically on the trailing edge of endplates, can increase Cl [18]. This can be useful when the rules regulate endplate size.

## 2.3 Wings on Cars

### 2.3.1 History

As presented by Zhang et al. [12], Figure 11 shows the evolution of wings on cars. Decreases in lap times were observed and continued as new types of aerodynamics were implemented. Regulations were quickly placed on aerodynamic components in the wake of many fatal crashes due to limited understanding of aerodynamic stability and component failure. All of these technologies, with the exception of powered aerodynamic devices, are still legal in SAE rules.

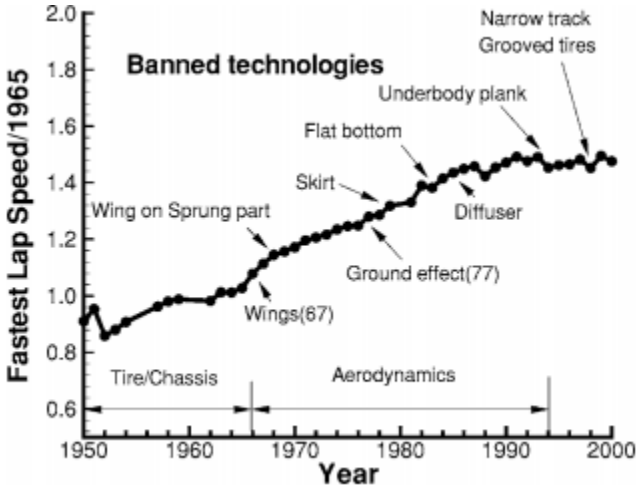


*Figure 11 Aerodynamic component's impact on lap times [12]*

Typical aerodynamic configurations of open wheel style cars include a front wing which operates in ground effect, an underbody which could include the floor of the car and/or tunnels with a rear diffuser that operates in ground effect, and a rear wing. Additional smaller aerodynamic components like strakes, vortex generators, and turning vanes have been seen recently and are used to control the air flow around the car. Again, the position and size of these components are strictly regulated by the rules. Unlike FSAE competitions, drag becomes a major concern because of high straight-line speed, fuel usage, and passing potential for other racing series.

### 2.3.2 Interactions Between Components

Race car aerodynamics are unique because of the close proximity of all the components. The close proximity between these components can lead to more complex aerodynamic interactions and is an area of research. This Section presents research conducted with regards to these interactions.

#### 2.3.2.1 Wheels and Tires

Zhang and Zerihan [14] present previous research with regards to front wheels and tires. Wheel and tire position negatively interferes with the flow structure of the front wing and components downstream like the underbody, side pods, and rear wing. Tire deformation, due to cornering forces, changes the flow structure around the wheels and tires and affects aerodynamic components, noting a 5% reduction in downforce when the tire is deformed [19], [20], [21], [22]. Sprot et al. [21] studies ways to change flow structure around the wheels and tires with ducting, integrated into the wheel assembly.

2.3.2.2 Front Wing Wake

Zhang and Zerihan [11] study the front wing wake of a single element wing in ground effect using a wind tunnel. At large h/c values the front wing wake was small with low turbulence resulting in good downstream flow but a low front wing Cl. Lower h/c values produced a large wake with high turbulence and mixing. This configuration had a higher front wing Cl but could affect downstream components depending on their location.

Wordley and Saunders [7] present wind tunnel data from a complete FSAE car on the effect the front wing wake has on rear wing Cl and Cd. As shown in Figure 12, rear wing Cl increases of 1.5 were seen when the rear wing was raised from 1050 mm to 1470 mm. This is evidence on the negative influence the front wing wake on the rear wing Cl. Raising the rear wing is an effective way to increase rear wing Cl without adding weight.

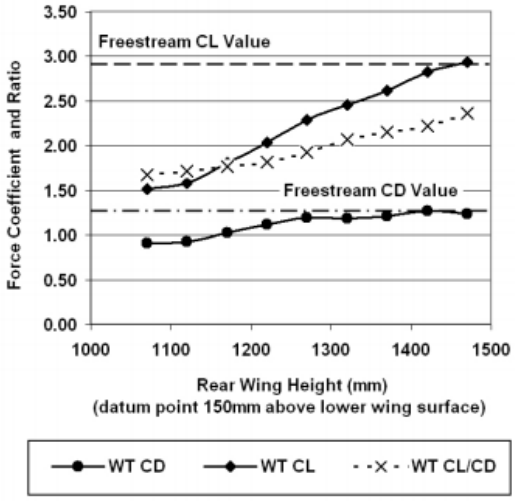


*Figure 12 Effect of front wing wake on rear wing [7]*

Zhang and Zerihan [23] study vortex formation and its effect on a two element front wing in ground effect using a wind tunnel. The flow on main element was shown to be highly 3 dimensional, influenced by an edge vortex. Again, this flow has an influence on downstream components and should be considered during the design of the complete car.

2.3.2.3 Rear Wing and Underbody Interaction

Many racecars are seen with a low rear wing, sometimes referred to as a beam wing, positioned above the underbody exit. Katz [5], McBeath [6], and Katz and Dykstra [24] show that the addition of a rear wing and its angle can increase underbody Cl.

2.3.2.4 Yaw

Yaw is studied to understand how Cl, Cd, Cl/Cd, and center of pressure of the wings and the car changes when the car is turning or sliding. This is particularly important to FSAE because the courses consist mostly of corners. There is limited available research on cars in yaw because of the increased model complexity, computational time, and ability to physically validate the results. Wordley and Saunders [7] present wind tunnel data from a multi element wing in free stream at different yaw angles, shown in Figure 13. Cl decreases with increased yaw angle, more abruptly at angles higher than 25 degrees.

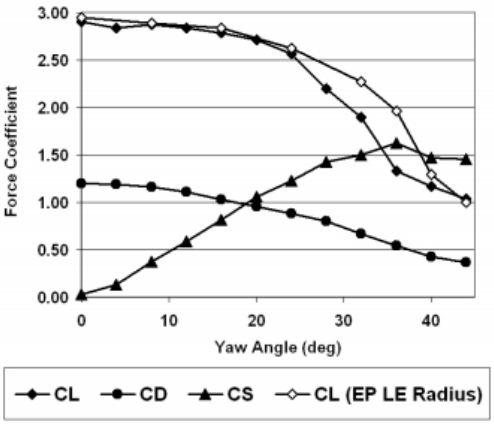


*Figure 13 Cl vs yaw angle for a wing in free stream [7]*

Cañada [25] also notes a drop in Cl with increased yaw angle. Figure 14 shows separation off on leading edge of endplate similar to [7].

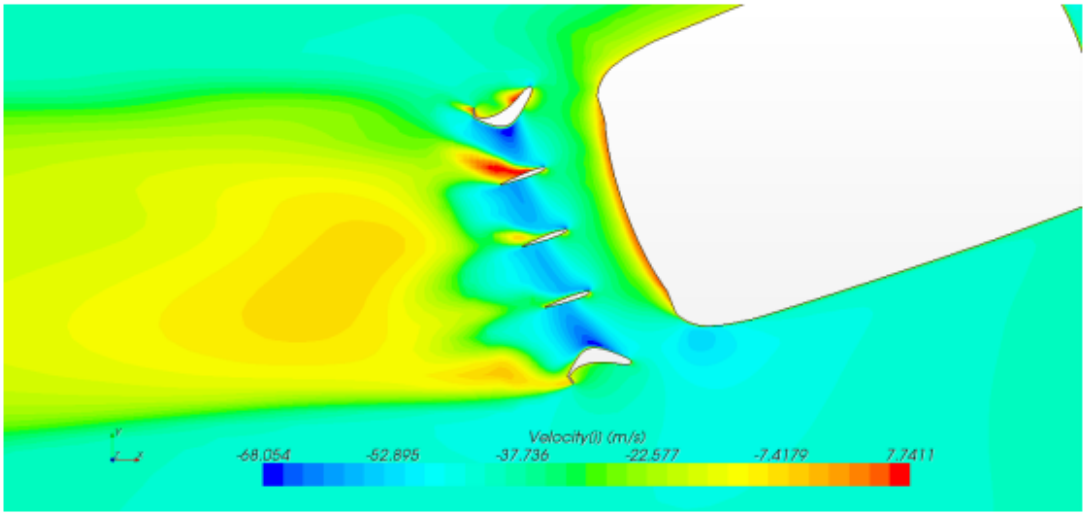


*Figure 14 Velocity distribution of rear wing in yaw (top view) [25]*

Roberts et al. [26] presents wind tunnel results of an isolated front wing in ground effect at yaw angles up to 5 degrees shown in Figure 15. A small decrease in Cl and Cd is observed at h/c < 0.20. Here, downforce is reported by a negative coefficient of lift.

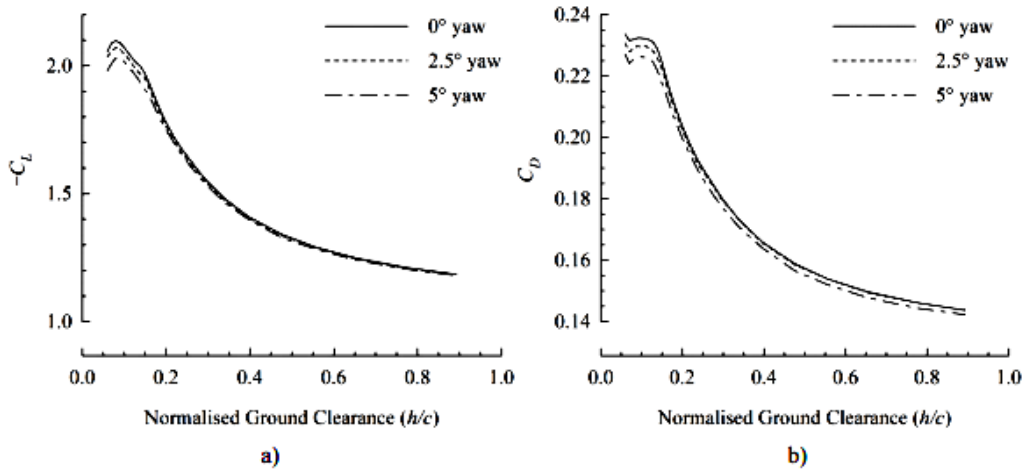


*Figure 15 Front wing in yaw [26]*

2.3.2.5 Working Within the Rules

Most racing series regulate the size and position of aerodynamic components. Gopalarathnam and Selig [27] makes suggestions for angle of attack, main element chord length and flap chord length, and slot gap to maximize Cl for a two element wing when constrained to a particular volume.

2.3.2.6 Power Absorbed

Power absorbed, defined in Equation 12, is a measure of the power needed to overcome an aerodynamic drag force. A car is said to be "drag limited" when it can no longer increase its longitudinal speed. This occurs when power absorbed is equal to the maximum engine power.

$$Power\ Absorbed = \frac{CdA_f v^3 \rho}{2} \tag{12}$$

It is important to note that power absorbed is related to $v^3$. The low speeds in FSAE reduce the chance of the car being drag limited.

2.4 Need for Research

Research presented in Section 2 gives some guidelines for race car aerodynamic design. Much of this research is limited to isolated wings without the complete car. There is a lack of available research on how multiple wings on a car effect each other and general guidelines for their positions and angles when designing for overall Cl, Cd, Cl/Cd, and center of pressure.

This thesis aims to fill in the gaps in current research by using CFD simulations to study the interactions between each wing on a complete car. Conclusions can be made based on trends from sensitivity studies to aid designers with the multiple objectives in the FSAE competition.

2.5 Objective Review

Table 1 provides an overview of SAE events with respect to downforce and drag. Minimum weight is desired for all dynamic events and the goal is to score as many points as possible. It is clear that for almost every event downforce should be increased. However, as presented in Section 2.2.3, downforce and drag are coupled so a balance between downforce and drag must be considered.

| **Event** | **Downforce** | **Drag** | **Notes** |
|---|---|---|---|
| *Design* | n/a | n/a | Provide justification |
| *Cost* | n/a | n/a | Minimize cost, reduce area |
| *Presentation* | n/a | n/a | Adds value |
| *Acceleration* | Increase | Decrease | Downforce has a very small effect. The goal should be to reduce as much drag as possible |
| *Skidpad* | Increase | n/a | Maximum downforce configuration |
| *Autocross* | Increase | Decrease | Maximum downforce configuration while limiting drag |
| *Endurance* | Increase | Decrease | Maximum downforce configuration while limiting drag |

| | | | |
|---|---|---|---|
| *Efficiency time* | Increase | Decrease | Tradeoff with efficiency fuel |
| *Efficiency fuel* | Decrease | Decrease | Tradeoff with efficiency time |

*Table 1 Objective summary*

# 3. COMPUTATIONAL FLUID DYNAMICS SIMULATION

## 3.1 Computational Fluid Dynamics Model

CFD simulations were used to conduct a series of sensitivity studies. Star CCM+, by CD-adapco, was the chosen software based on its availability and support for FSAE teams. A half car model, with a symmetry plane on the car's xz plane, was built. Ahmad and Abo-Serie [28] concluded the half car simulation's downforce accuracy was within 0.84% compared to a full car simulation. Using a half car model cuts the number of cells in the domain in half, decreasing required computing resources.

### 3.1.1 Wind Tunnel Configuration

Figure 16 shows the CFD model built, representing GFR's car in a typical straight-line driving condition without the influence of head, tail, or side wind. Table 2 shows the geometry of the wind tunnel and physics conditions for each wall. The wind tunnel was made large enough so the outer wall, ceiling, and outlet do not unintentionally affect the air flow around the car.

| **Dimension** | **Condition** | **Value** |
|---|---|---|
| Length | - | 60 m |
| Width | - | 10 m |
| Height | - | 10 m |
| Inlet | Velocity inlet | 65 kph |
| Outlet | Pressure outlet | 0 gauge |
| Floor | Wall - velocity | 65 kph |
| Ceiling | Wall | - |
| Outer wall | Wall | - |
| Center wall | Symmetry plane | Slip |

*Table 2 Wind tunnel configuration*

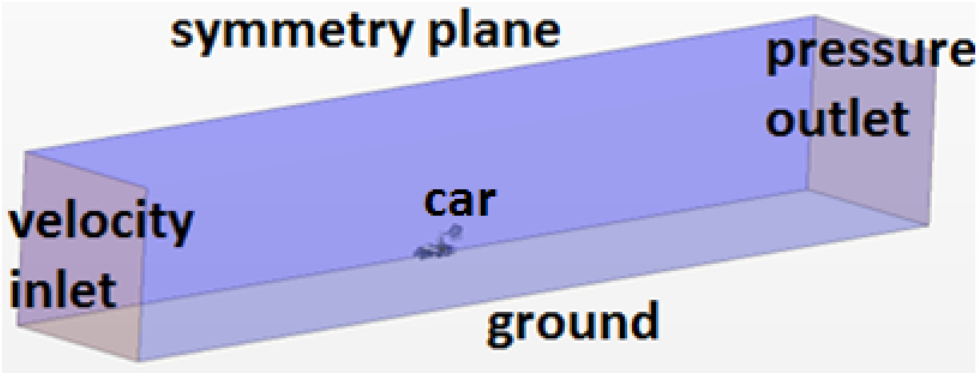


*Figure 16 Wind tunnel configuration*

### 3.1.2 Mesh Convergence

Three different mesh densities, coarse, medium, and fine, were generated to test mesh convergence. The results are presented in Table 3. Residuals approach E-4 for the coarse mesh and trend below E-4 for the medium and fine meshes as seen in Figure 18, 20, and 22. All mesh densities achieved stability in downforce and drag values as seen in Figure 17, 19, and 21, and. Iterations to converge and time per iteration increased with increased mesh densities. Tradeoffs with mesh density, Cl and Cd error, and run time should be considered in design of experiment. Without knowledge of the exact solution it is impossible to determine true error. The medium mesh density produced Cl and Cd values 64.2% faster and within 1% of the fine mesh. Considering the resources available, a medium mesh density was chosen and will allow for more simulations with reasonable error.

| **Mesh Density** | **Cell count** | **Iterations to converge** | **Time / iteration** | **Run time** | **Cl** | **Cl error** | **Cd** | **Cd error** |
|---|---|---|---|---|---|---|---|---|
| Coarse | 1248317 | 700 | 9.86 sec | 115.03 min | 4.314 | -5.06% | 2.013 | 0.15% |
| Medium | 5439691 | 960 | 48.65 sec | 778.40 min | 4.534 | -0.22% | 2.035 | 0.94% |
| Fine | 6888954 | 1600 | 81.52 sec | 2173.87 min | 4.544 | - | 2.016 | - |

*Table 3 Mesh convergence*

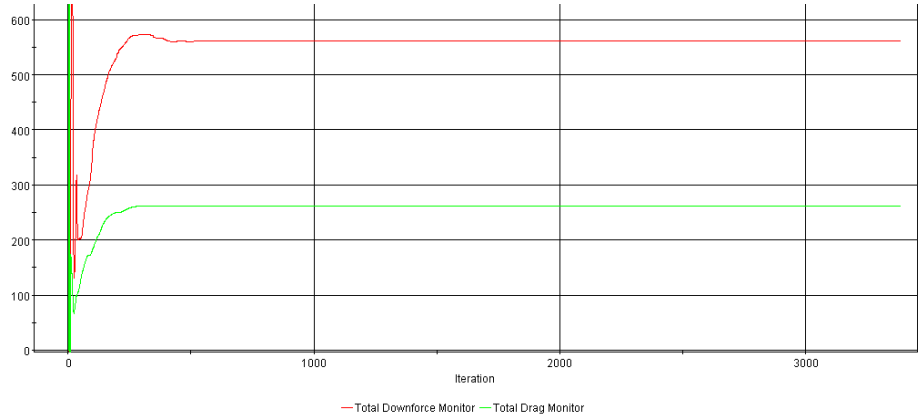


*Figure 17 Downforce and drag for coarse mesh*

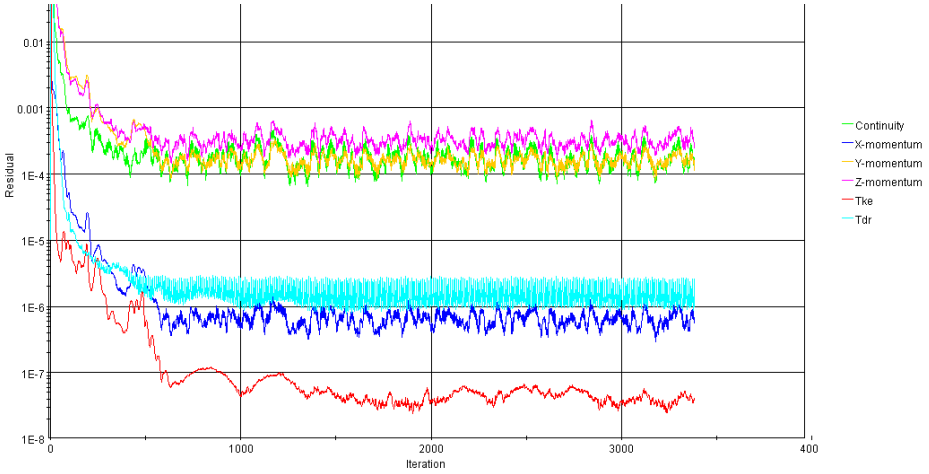


*Figure 18 Residuals for coarse mesh*

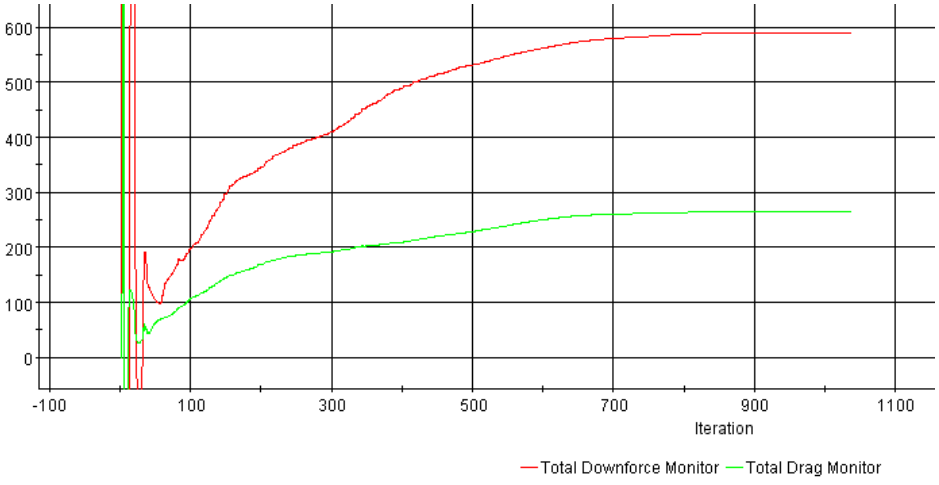


*Figure 19 Downforce and drag for medium mesh*

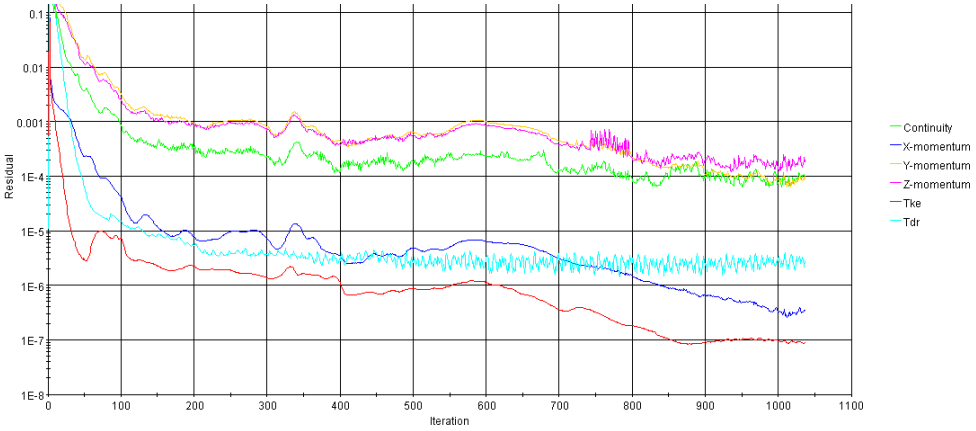


*Figure 20 Residuals for medium mesh*

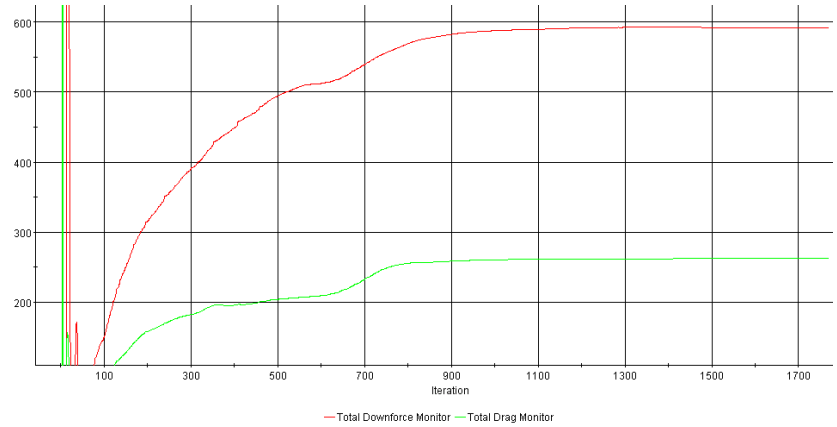


*Figure 21 Downforce and drag for fine mesh*

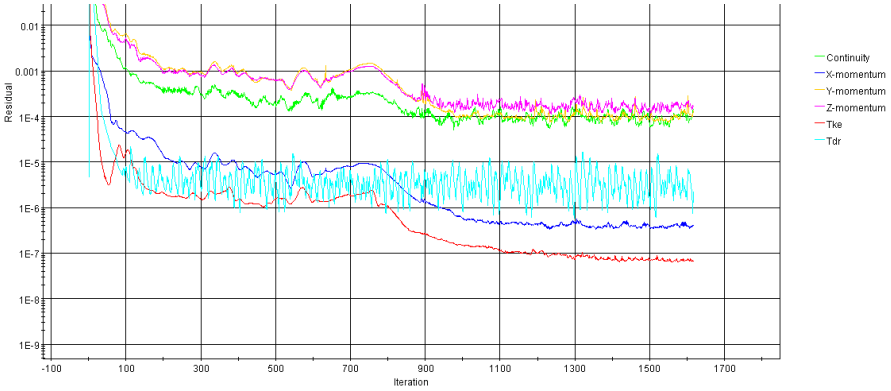


*Figure 22 Residuals for fine mesh*

### 3.1.3 Mesh Settings

Mesh settings, shown in Table 4, 5, 6, 7, and 8 were chosen based on suggestions from CD-adapco [29] and research within the team. Volumetric controls, shown in

Figure 23, 24, 25, and 26 were used for local mesh refinement in areas with high pressure gradients.

| Setting | Value |
|---|---|
| Mesh | Trimmer |
| Cell count | ~5 million, depending on geometry |
| Base size | 1 m |
| Prism layers | 5 |
| Prism layer thickness | 10 mm |
| Prism layer stretching | 1.5 |
| Surface size | Min .5 m, target 1m |

*Table 4 Mesh settings for wind tunnel volume*

| Setting | Value |
|---|---|
| Custom size | 30 mm |
| Prism layers | 8 |
| Prism layer thickness | 10 mm |
| Prism layer stretching | 1.5 |

*Table 5 Mesh settings for car volumetric control*

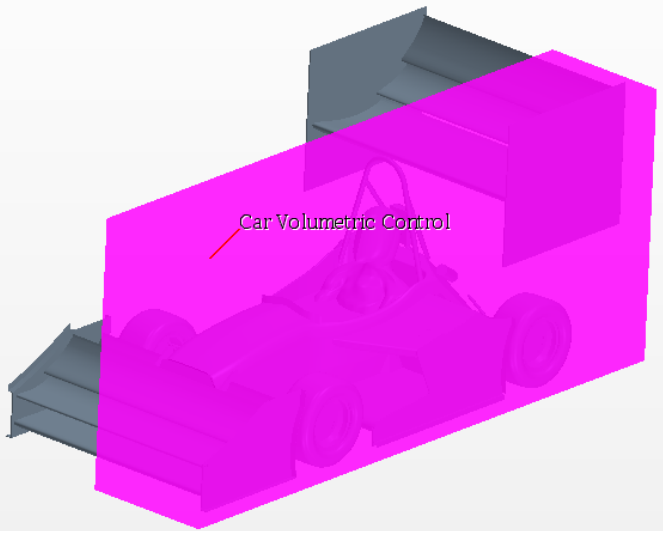


*Figure 23 Car volumetric control*

| Setting | Value |
|---|---|
| Custom size | 10 mm |
| Prism layers | 10 |
| Prism layer thickness | 5 mm |
| Prism layer stretching | 1.5 |

*Table 6 Mesh settings for front wing volumetric control*

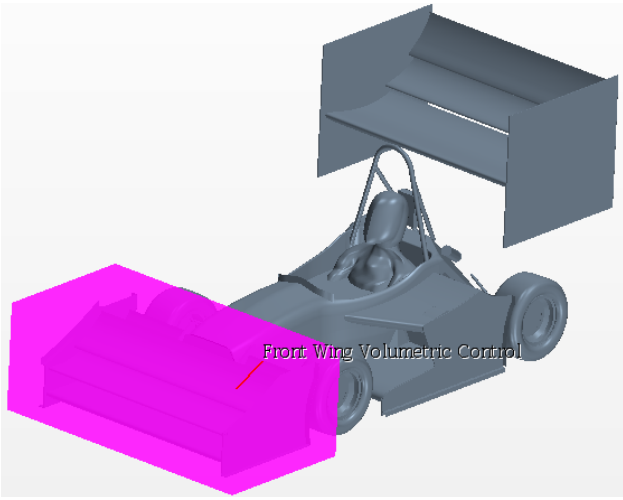


*Figure 24 Front wing volumetric control*

| **Setting** | **Value** |
|---|---|
| Custom size | 10 mm |
| Prism layers | 10 |
| Prism layer thickness | 5 mm |
| Prism layer stretching | 1.5 |

*Table 7 Mesh settings for undertray volumetric control*

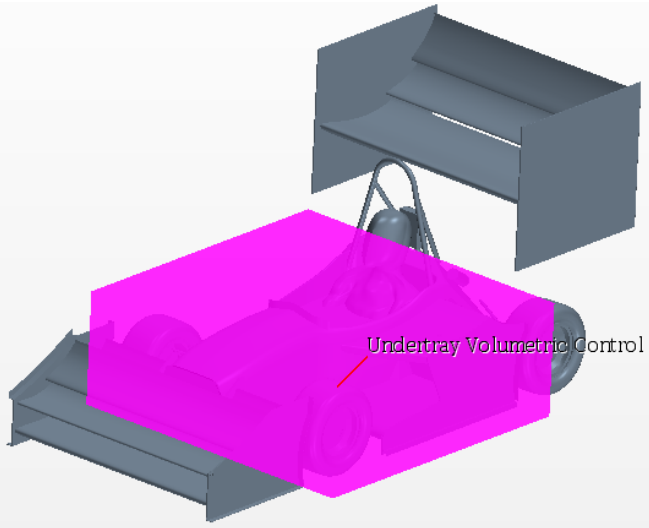


*Figure 25 Undertray volumetric control*

| **Setting** | **Value** |
|---|---|
| Custom size | 10 mm |
| Prism layers | 10 |
| Prism layer thickness | 5 mm |
| Prism layer stretching | 1.5 |

*Table 8 Mesh settings for rear wing volumetric control*

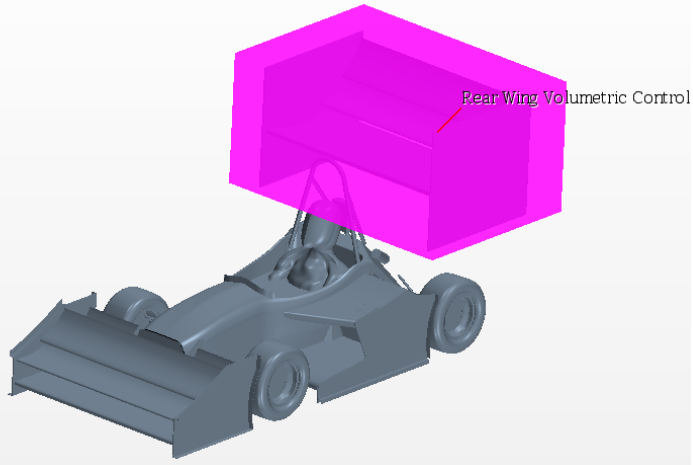


*Figure 26 Rear wing volumetric control*

### 3.1.4 Physics Model

Physics models, shown in Table 9, were chosen based on suggested by CD-adapco [29] and research within the team.

| | |
|---|---|
| Turbulence | K-Epsilon |
| Solver | Segregated flow |
| Gas | Incompressible [30] |
| Time | Steady |
| Space | Three dimensional |

*Table 9 Physics models*

### 3.1.5 Included Parts

As many parts as possible were included in the simulations to increase model accuracy as noted in Table 10. Figure 27, 28, and 29 show the general geometry of the car.

| **Part** | **Comment** |
|---|---|
| Chassis | Filled without engine openings |
| Driver | With helmet |
| Headrest | Minimum per rules |
| Suspension | Simplified |
| Wheels | Simplified and rotating at ground speed |
| Wing mounts | None, not designed at time of simulation |

*Table 10 CFD car parts*

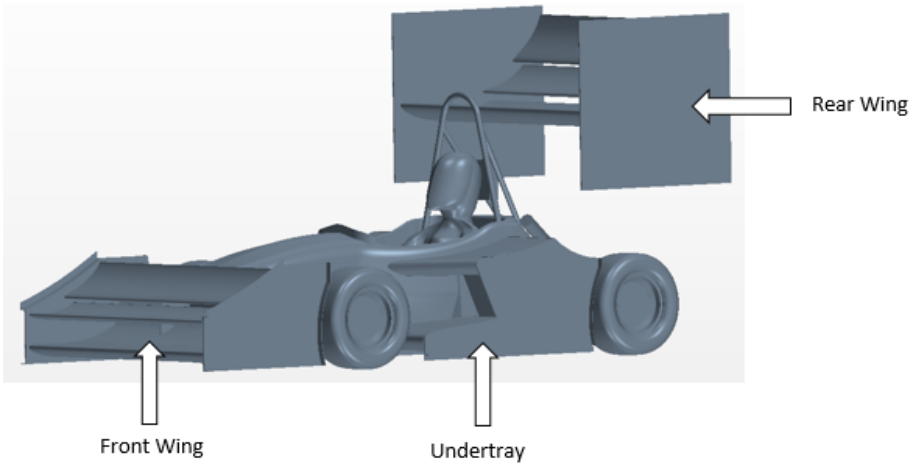


*Figure 27 CFD car model isometric view*

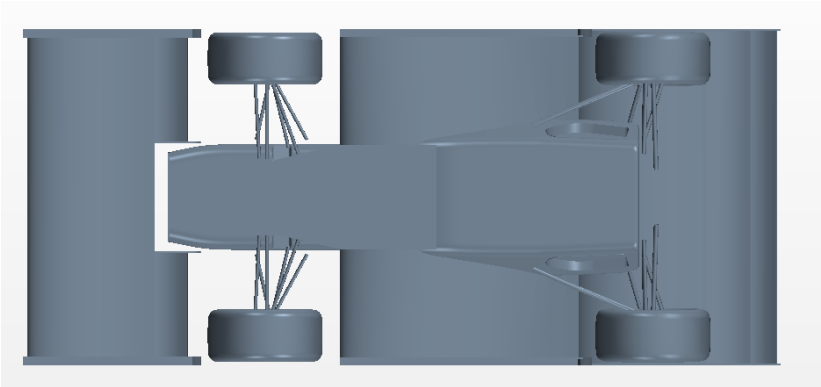

*Figure 28 CFD car model bottom view*

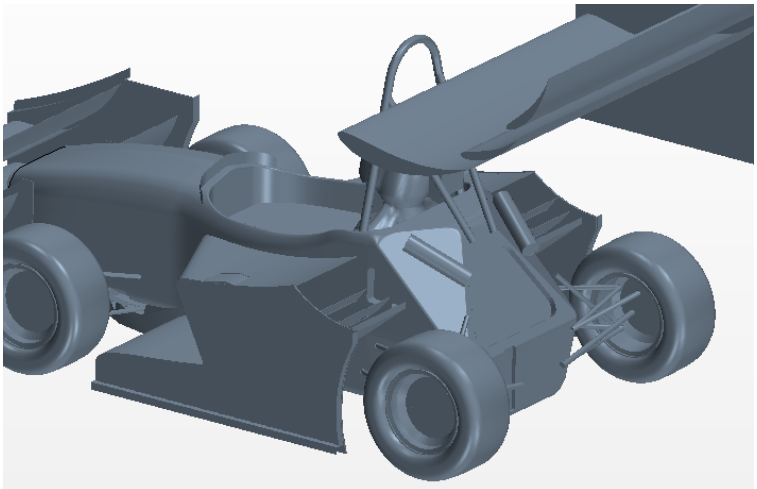

*Figure 29 CFD car model rear view*

# 4. COMPUTATIONAL FLUID DYNAMICS RESULTS

Using the CFD model presented in Section 3, Section 4 will conduct three different sensitivity studies. By varying the position and angle of different wings, trends in Cl, Cd, Cl/Cd, and center of pressure can be observed.

## 4.1 Front Wing Height Study

In this study, the complete front wing (including endplates) varies in height from h/c = 0.180 to 0.038. The range of heights chosen cover the heights presented by Zhang and Zerihan [14] and can be applied to the actual design of GFR's car. The objective of this study is to identify trends in Cl, Cd, Cl/Cd, and center of pressure for different aerodynamic components and the complete car.

Figure 30 shows the front wing used in this study. Figure 31 shows the full car configuration. Table 11 shows the relevant wing geometry.

| **Parameter** | **Value** | **Unit** |
|---|---|---|
| Height/Chord | 0.180-0.038 | n/a |
| Main Element | | |
| Thickness | 12 | % chord |
| Camber | 10 | % chord |
| Angle of attack | 10 | degrees |
| Flap | | |
| Thickness | 12 | % chord |
| Camber | 10 | % chord |
| Angle of attack | 36 | degrees |
| Endplate | | |
| Footplate | 30 | mm |
| Vertical Gurney | 30 | mm |
| Upper Gurney | 30 | mm |

*Table 11 Front wing configuration*

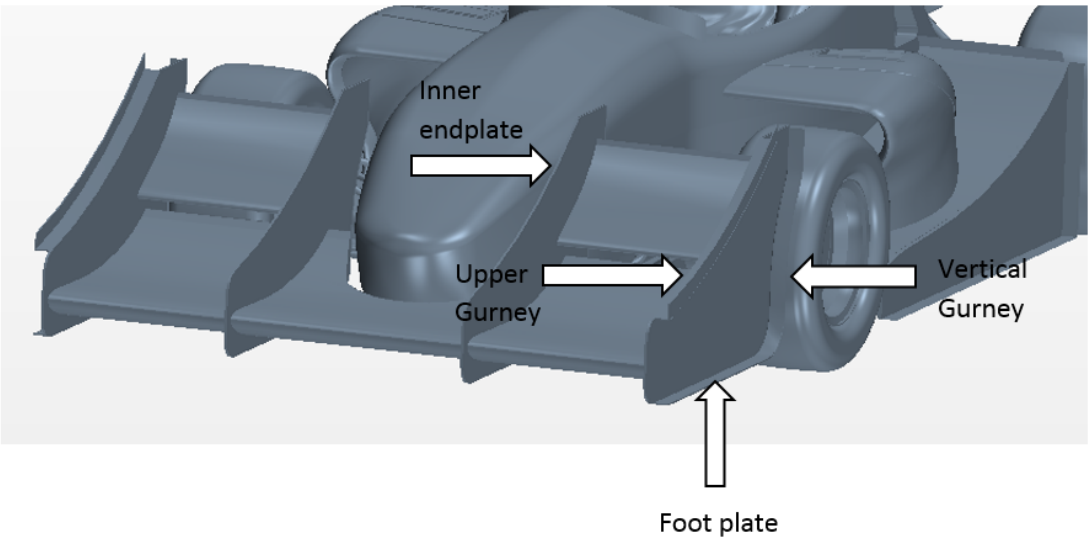


*Figure 30 Front wing configuration*

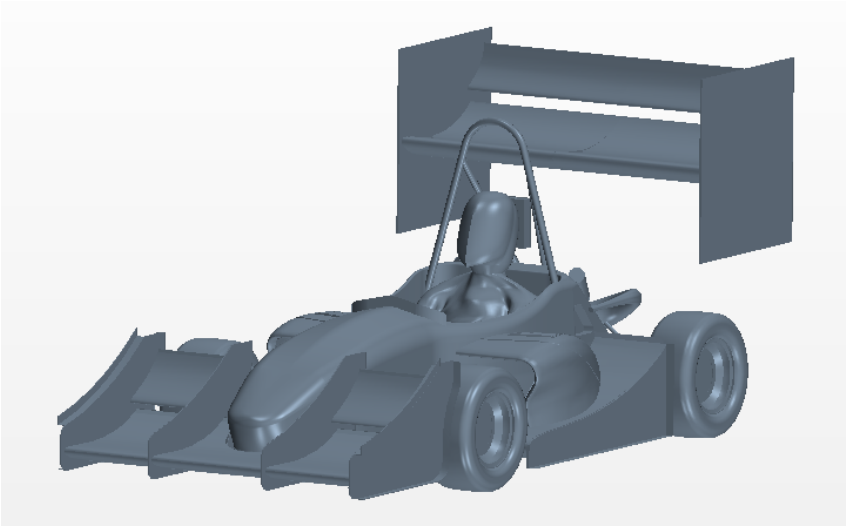

*Figure 31 Full car configuration*

### 4.1.1 Effect on Front Wing

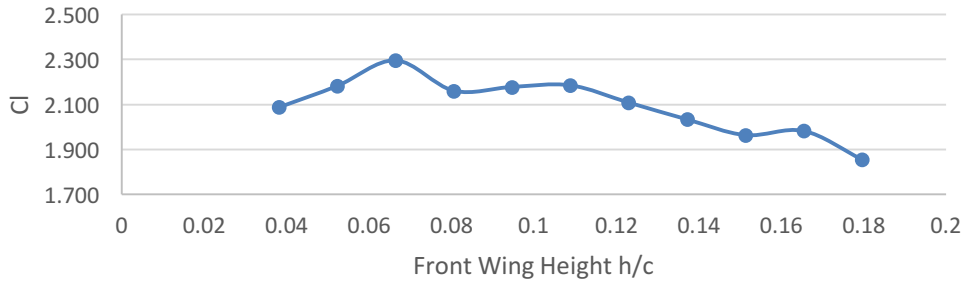


*Figure 32 Front wing Cl vs front wing height*

Figure 32, consistent with [14], shows a trend of increasing front wing Cl with decreasing height until h/c = 0.066. The drop in Cl below h/c = 0.066 is not as sharp compared to [13] and [14]. The increase in Cl is substantial, more than 23% from h/c = 0.180 to h/c = 0.066. This data shows that reducing front wing height is an easy way to increase front wing Cl without additonal weight.

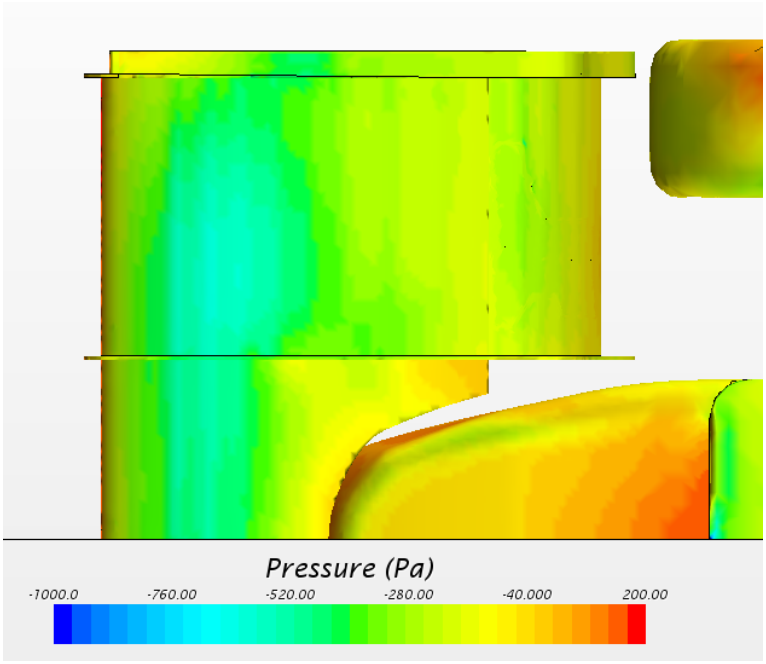


*Figure 33 Pressure distribution of front wing at h/c = 0.080*

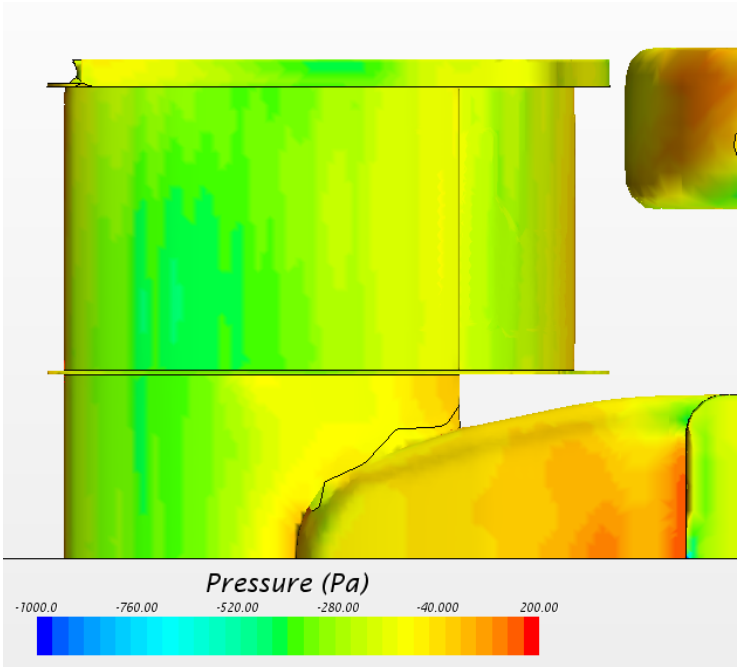


*Figure 34 Pressure distribution of front wing at h/c = 0.165*

Figure 33 and 34 show lower pressure on the bottom of the front wing main element and flap at h/c = 0.080 and h/c = 0.165. The lower pressure in Figure 33 is consistent with the increase in Cl in the h/c = 0.080 configuration.

As the rules allow front wings up to 30 inches in front of the front tires, small variations in pitch could affect front wing height and resultant aerodynamic forces dramatically. Additionally, as per FSAE Rule T6.2, the wing must not touch the ground. The designer should take these considerations into account when selecting front wing h/c.

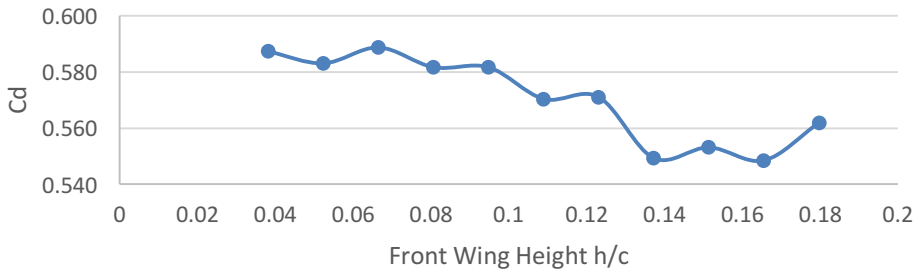


*Figure 35 Front wing Cd vs front wing height*

Figure 35 shows that front wing Cd also follows a similar trend to [14] increasing as height is reduced. A maximum Cd value is at h/c = 0.066, decreasing slightly as h/c decreases further. The increases in Cd are proportionally smaller than the increases in Cl, only 7.3%. The increase in front wing Cd is not as linear and consistent compared to [14]. One expanation for this is the presence of the complete car and the interactions between the wheels and tires and other downstream components. The other explaination comes from the CFD model accuracy and inconsistencies with Star CCM+'s automated meshing. With this in mind, it is important to look for general trends over the range of samples and compare results with literature.

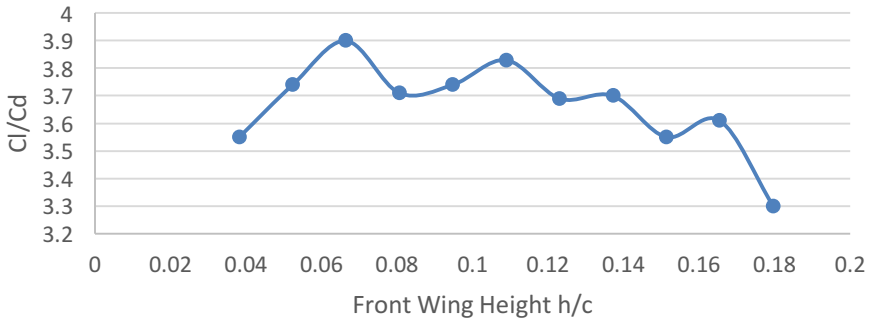


*Figure 36 Front wing Cl/Cd vs front wing height*

Figure 36 shows, that in general, front wing Cl/Cd increases as height is decreased, until a maximum at h/c = 0.066 is seen. Below h/c = 0.066, Cl/Cd decreases due to

the lower front wing Cl. This data shows it is possible to increase the front wing's Cl/Cd without additional weight.

### 4.1.2 Effect on Rear Wing

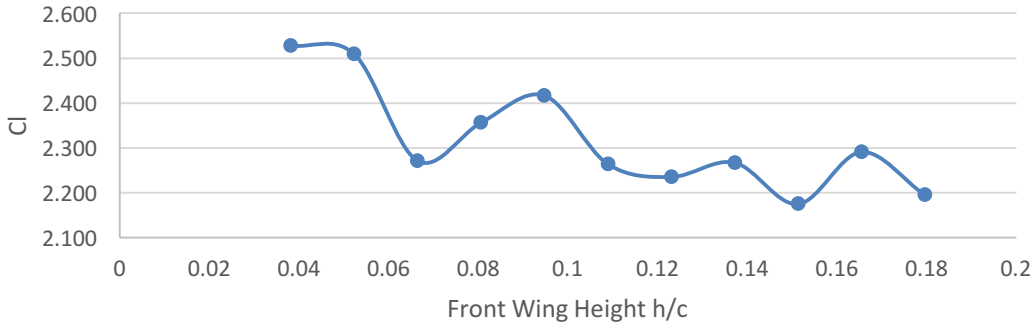


*Figure 37 Rear wing Cl vs front wing height*

Figure 37 shows a general trend of increasing rear wing Cl as the front wing is lowered. This shows the front wing is affecting the air flow to the rear wing. From this data one can conclude the rear wing is not in freestream, effected by the front wing's wake. Notably, the rear wing Cl increased by 16.2% between the minimum and maximum values. The inconsistency in rear wing Cl is the first example of the highly coupled aerodynamic system on the car. The rear wing is downstream and consequently affected by all other components. Figure 38 and 39 show the velocity distributions on the xz plane of the h/c = .080 and h/c = 0.165 configurations. Here, the wake of the front wing can be seen as well as the flow around the front wheels and tires. The flow direction of the air off the front wing is in an upwards direction. This is refereed to as up-wash. As the front wing is lowered, the up-wash has less of an effect on the incident angle of air to the rear wing. This supports the data shown in Figure 37.

If the designer's objective is to increase rear wing Cl, this data suggests reducing front wing height.

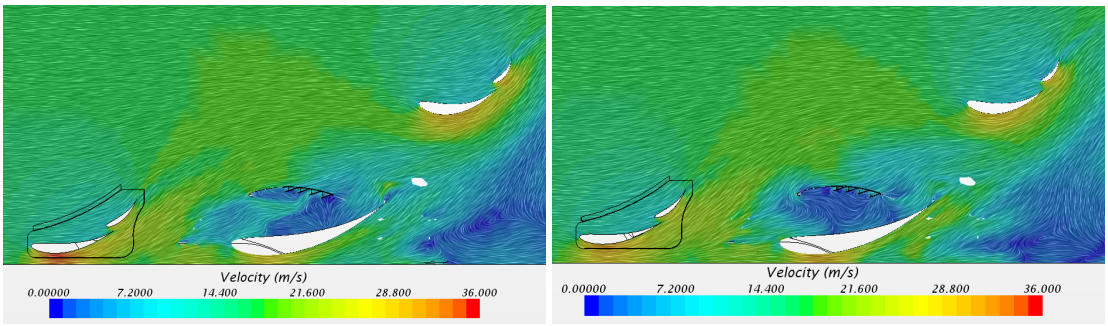


*Figure 38 Velocity distribution on the 0.35m xz plane at h/c = 0.080 (left) and h/c = 0.165 right*

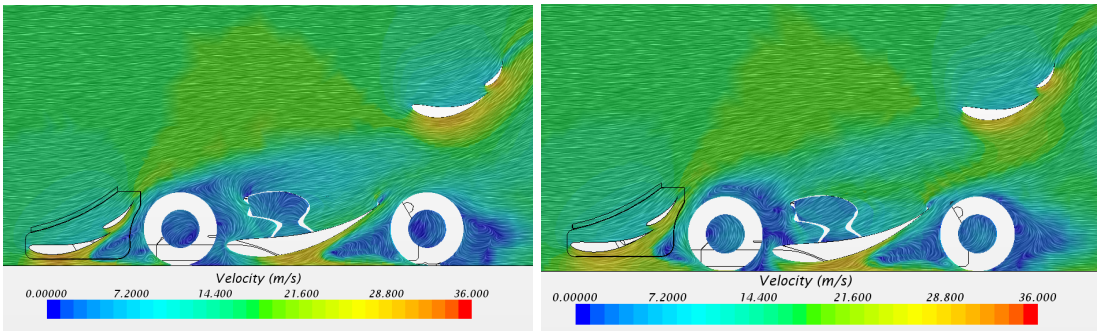


*Figure 39 Velocity distribution on the 0.55m xz plane at h/c = 0.080 (left) and h/c = 0.165 (right)*

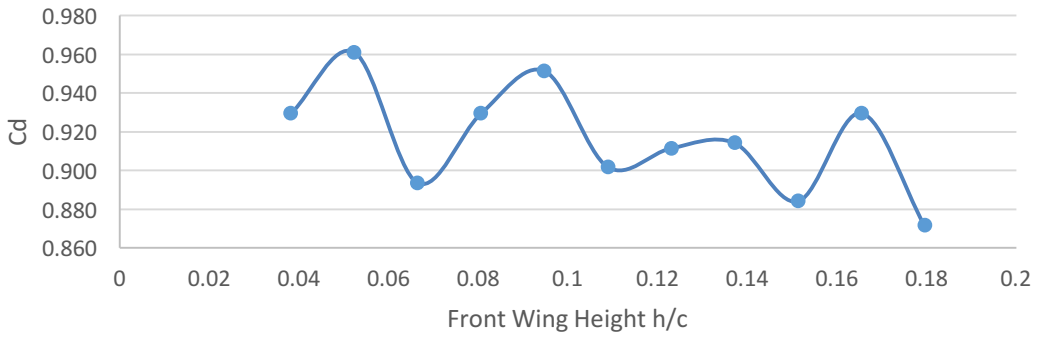


*Figure 40 Rear wing Cd vs front wing height*

Figure 40 shows that, in general, rear wing Cd follows a similar trend to the rear wing Cl, increasing as front wing height is decreased. The increase in rear wing Cd is likely vortex drag accompanied by the increase in the rear wing Cl. Notably, the rear wing Cd only increases by 10.2% between the minimum and maximum values.

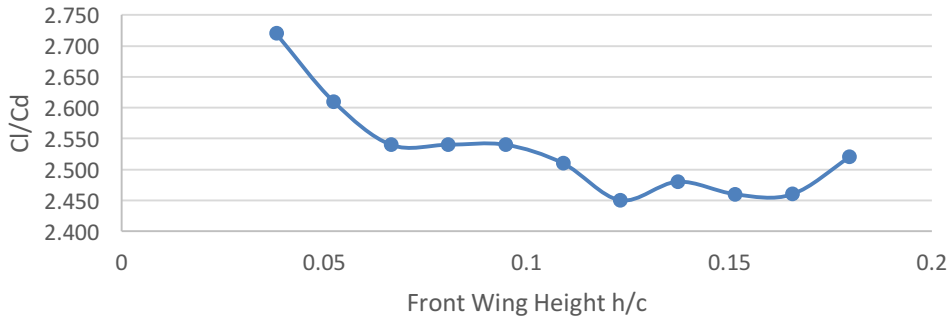


*Figure 41 Rear wing Cl/Cd vs front wing height*

Figure 41 shows an increasing Cl/Cd when the front wing is lowered. It supports Wordley and Saunders [7] claim that a higher small wing can produce more downforce and less drag than a large lower wing because of the influence of the front wing wake.

This would also be beneficial in FSAE because of the reduced weight of a smaller wing. If the objective is to increase rear wing Cl/Cd, front wing height should be reduced.

### 4.1.3 Effect on Undertray

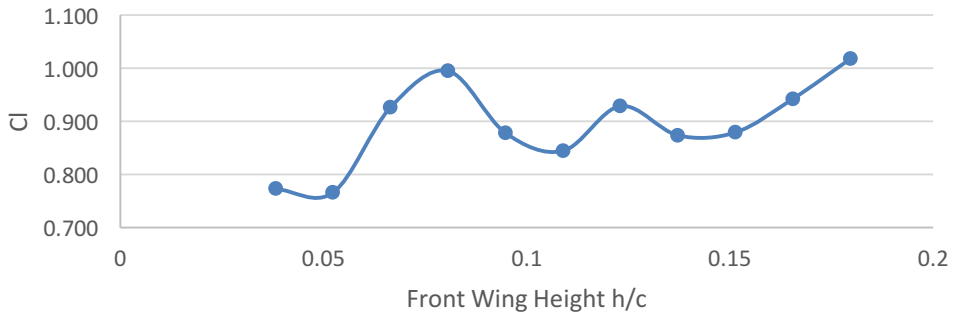


*Figure 42 Undertray Cl vs front wing height*

Figure 42 shows a trend of decreasing Cl with decreasing front wing height. As the undertray inlet height is 100mm off the ground, the decrease in front wing height affects the available air to the entry of the undertray. In this specific car configuration, the undertray is very close to the front wing and front wheels, likely increasing the negative effects of the front wing wake. This confirms the discussion in Section 2.3.2.2. Figure 43 and 44 show velocity distributions on the 0.35m xz plane. It is clear the up wash of the front wing in the h/c = 0.080 configuration is greater, resulting in less flow to the entry of the undertray.

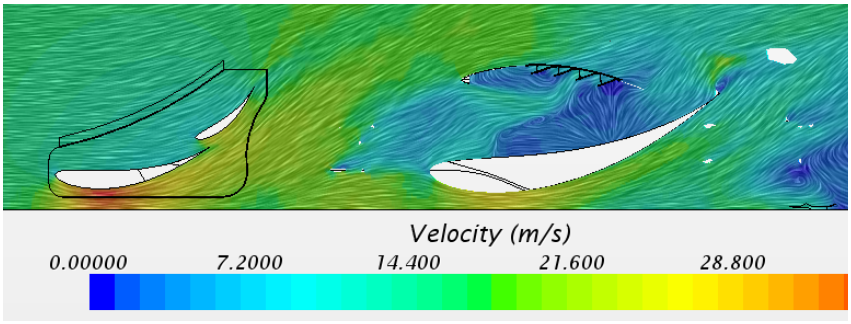


*Figure 43 Velocity distribution on the 0.35m xz plane at h/c = 0.080*

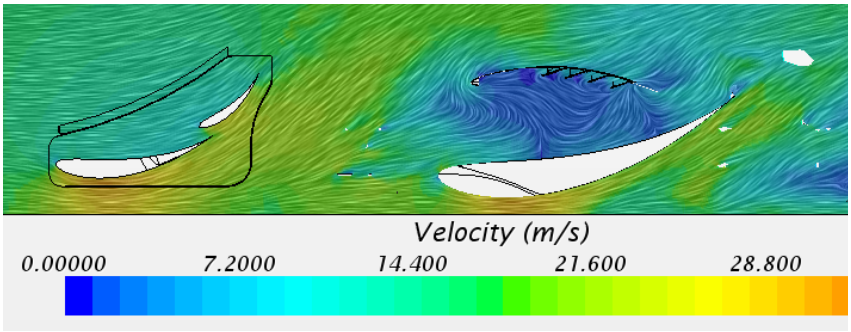


*Figure 44 Velocity distribution on the 0.35m xz plane at h/c = 0.165*

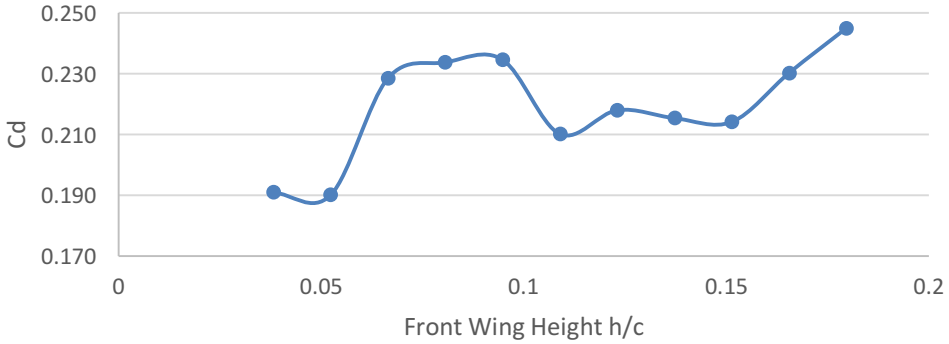


*Figure 45 Undertray Cd vs front wing height*

Figure 45 shows a decrease in undertray Cd is as front wing height is reduced. This is likely a reduction in vortex drag coupled with the decrease in undertray Cl.

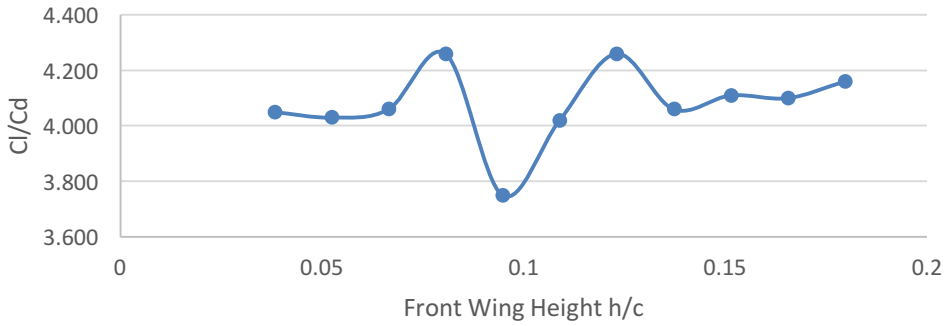


*Figure 46 Undertray Cl/Cd vs front wing height*

Figure 46 shows that Cl/Cd remains fairly constant except for a dip around h/c = 0.095. The Cl value at this height is larger and can be attributed to the front wing's interaction with the wheels and tires and close proximity to the undertray's entrance. This data supports [5] and [6] that the undertray can be the mostly efficient aerodynamic component on a car.

### 4.1.4 Effect on Front Wheels and Tires

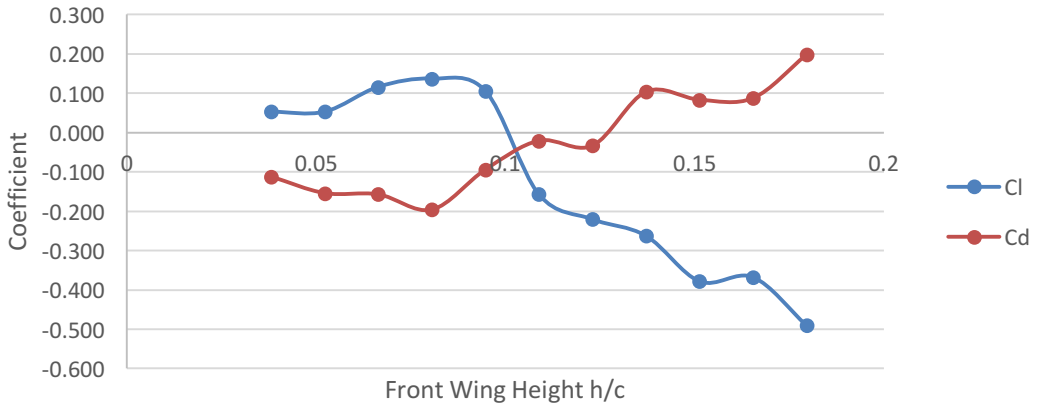


*Figure 47 Cl and Cd of front wheels and tires vs front wing height*

Figure 47 shows a trend of increasing front wheel and tire Cl and decreasing Cd with decreasing front wing height. Cd values trend below 0 at h/c = 0.105 contributing to forward force. The decrease in drag can be attributed to the change in flow and blockage around the front wheels and tires. At lower front wing heights, more air is directed above the wheels and tires rather than being trapped in the front lower half of the tires as shown by the pressure distribution in Figure 48. The endplate upper Gurney and endplate height can also be used to control the tip vortex around the top or side of the tire as seen in Figure 49.

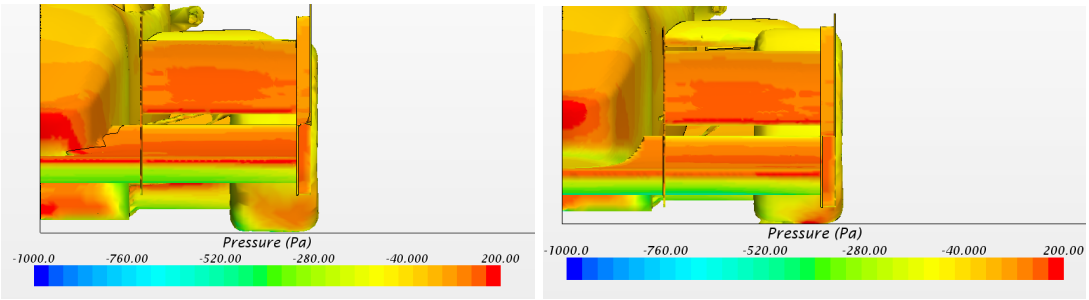


*Figure 48 Pressure distribution of front tire at h/c = 0.165 (left) and h/c = 0.080 (right)*

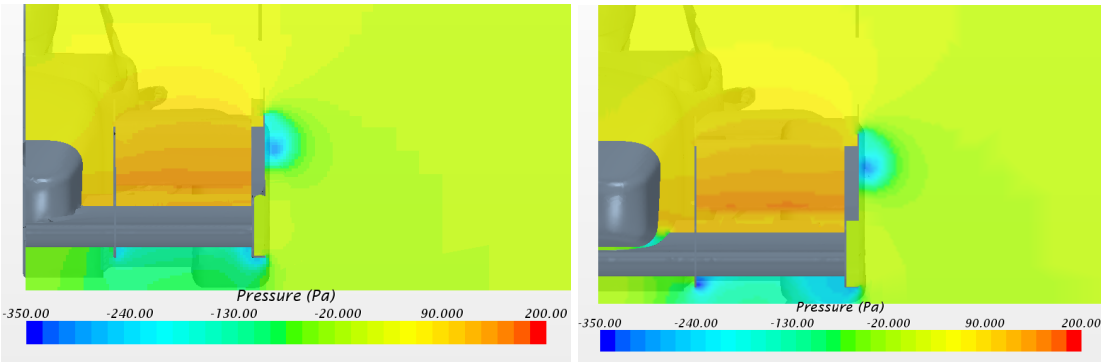


*Figure 49 Pressure distribution on -0.5m yz plane at h/c = 0.165 (left) and h/c = 0.080 (right)*

Figure 49 shows lower pressure beneath front wing main element and stronger tip vortices off bottom outer and inner endplates at h/c = 0.080. There is a similar strength tip vortex off upper outer endplate in the h/c = 0.165 and h/c = 0.080 configurations.

### 4.1.5 Effect on Full Car

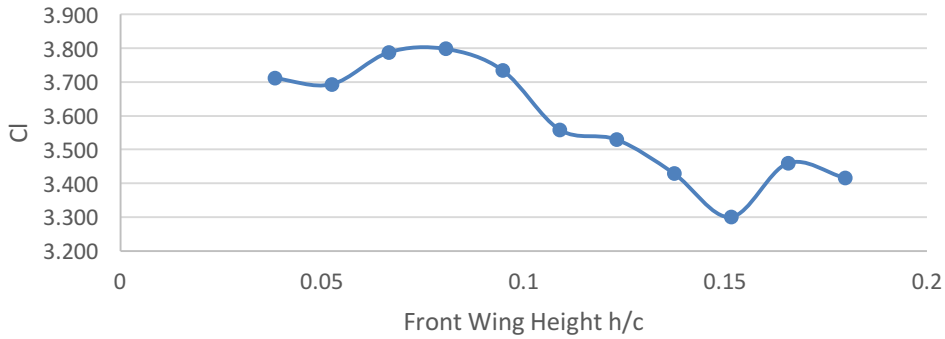


*Figure 50 Full car Cl vs front wing height*

Figure 50 shows a maximum full car Cl of 3.80 at h/c = 0.080. The decrease below h/c = 0.066 can be attributed to the decrease in front wing Cl as the front wing is too low to the ground and loses downforce.

The curve follows the trend that decreasing front wing height to h/c = 0.080 will increase full car Cl. Full car Cl can be increased by 15% without additional weight by positioning the front wing at the correct height.

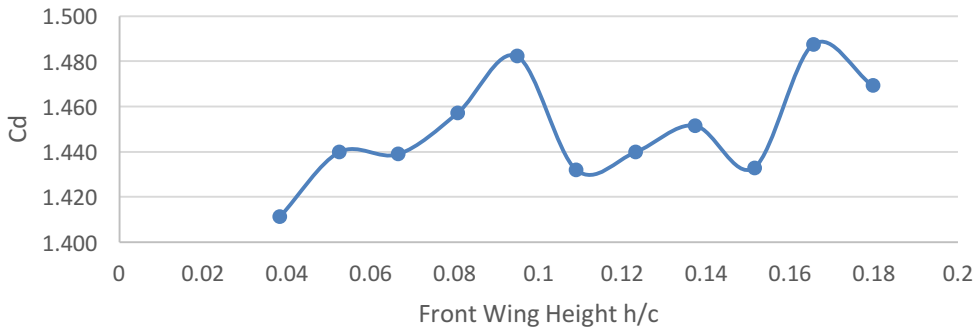


*Figure 51 Full car Cd vs front wing height*

Interestingly, Figure 51 shows the full car Cd follows a decreasing trend as front wing height decreases. Opposite to the front wing and rear wing, the undertray and front wheels and tires Cd decreased at lower front wing heights resulting in a lower overall Cd. Overall a 5.2% decrease in full car Cd is seen between the minimum and maximum values.

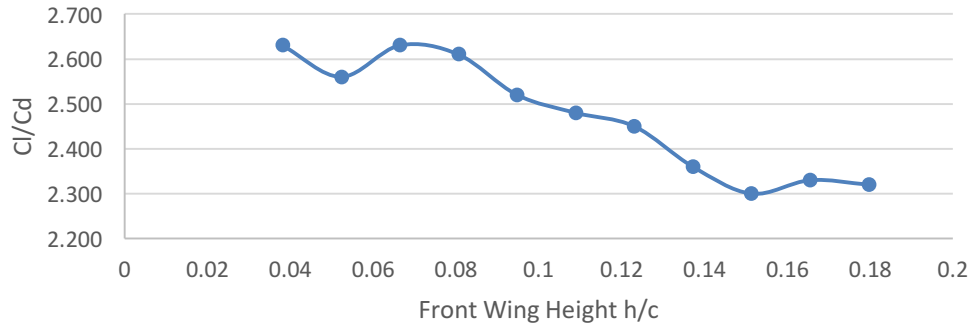


*Figure 52 Full car Cl/Cd vs front wing height*

Figure 52 shows that the Cl/Cd curve has a maximum value at h/c = 0.038 and h/c = 0.066 with a trend of increasing Cl/Cd as front wing height is decreased. If the objective is to increase Cl/Cd of the car, front wing h/c should be in this range.

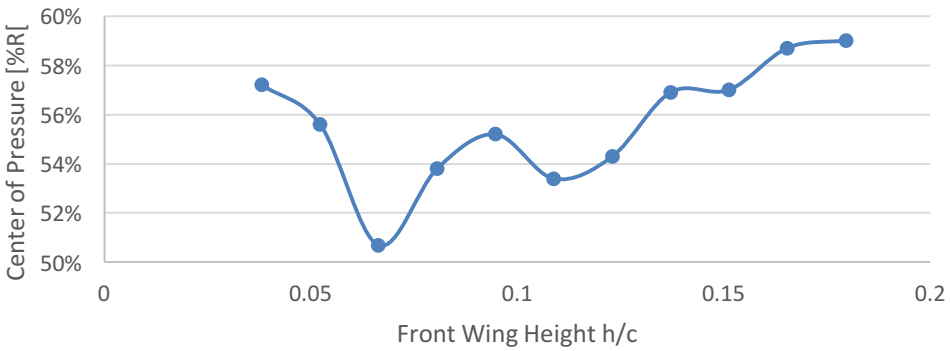


*Figure 53 Center of pressure vs front wing height*

Figure 53 shows that center of pressure moves forward as front wing height decreases caused by the large increase in front wing Cl until h/c = 0.066. The center of pressure then moves rearwards below h/c = 0.066 as front wing is too close to the ground resulting in lower front wing Cl. The balance change is fairly significant, moving up to 8% forward. Depending on vehicle center of gravity, other adjustments may have to be made to achieve the target center of pressure.

Table 12 summarizes the general trends of the front wing height study as h/c is reduced.

| **Part** | **Cl** | **Cd** | **Cl/Cd** |
|---|---|---|---|
| Front Wing | Increased | Increased | Increased |
| Rear wing | Increased | Increased | Increased |
| Undertray | Decreased | Decreased | No change |
| Full Car | Increased | Decreased | Increased |

*Table 12 Front wing height study summary*

## 4.2 Front Wing Flap Angle of Attack Study

In this study, the front wing flap angle of attack varies from 36 degrees to 48 degrees. The objective is to identify trends in Cl, Cd, Cl/Cd, and center of pressure for different aerodynamic elements and of the complete car. The flap was rotated about its leading edge to limit the effect of slot gap variation.

Figure 54 and 55 show the front wing used in this study. Figure 56 shows the full car configuration. Table 13 shows the relevant wing geometry.

| Parameter | Value | Unit |
|---|---|---|
| Main Element | | |
| Thickness | 12 | % chord |
| Camber | 10 | % chord |
| Angle of attack | 10 | degrees |
| Height/Chord | .080 | n/a |
| Flap 1 | | |
| Thickness | 12 | % chord |
| Camber | 10 | % chord |
| Angle of attack | 36-48 | degrees |
| Flap 2 | | |
| Thickness | 12 | % chord |
| Camber | 10 | % chord |
| Angle of attack | 10 | degrees |
| Flap 3 | | |
| Thickness | 12 | % chord |
| Camber | 10 | % chord |
| Angle of attack | 36 | degrees |
| Endplate | | |
| Height off ground | 32 | mm |
| Footplate | 30 | mm |
| Vertical Gurney | 30 | mm |
| Upper Gurney | 30 | mm |

*Table 13 Front wing configuration*

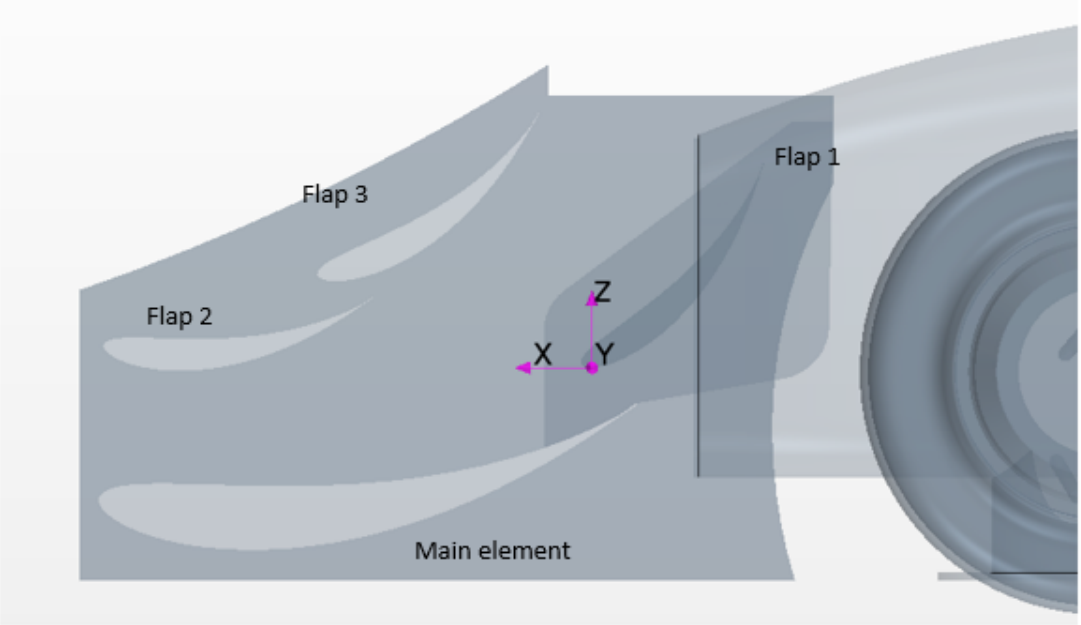


*Figure 54 Front wing configuration and flap rotation axis*

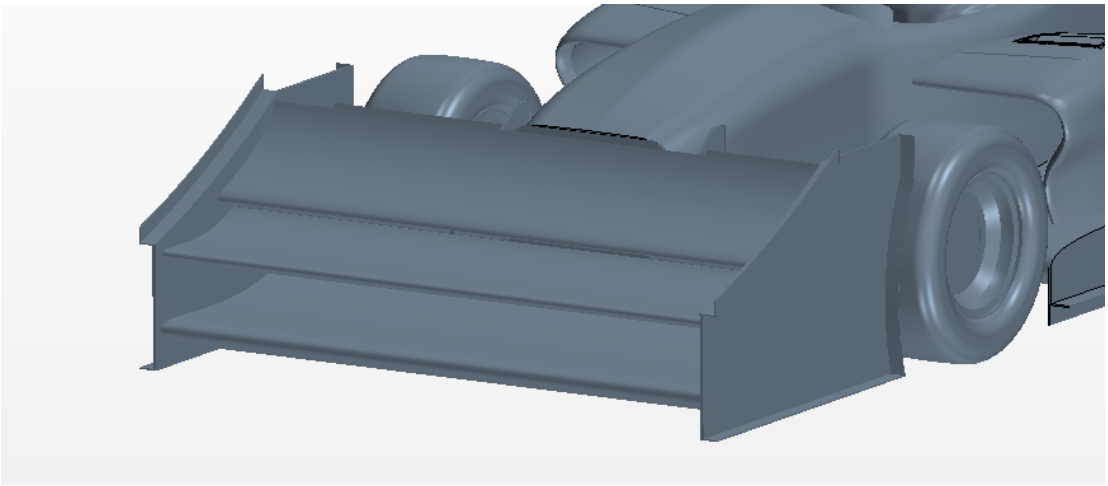

*Figure 55 Front wing configuration*

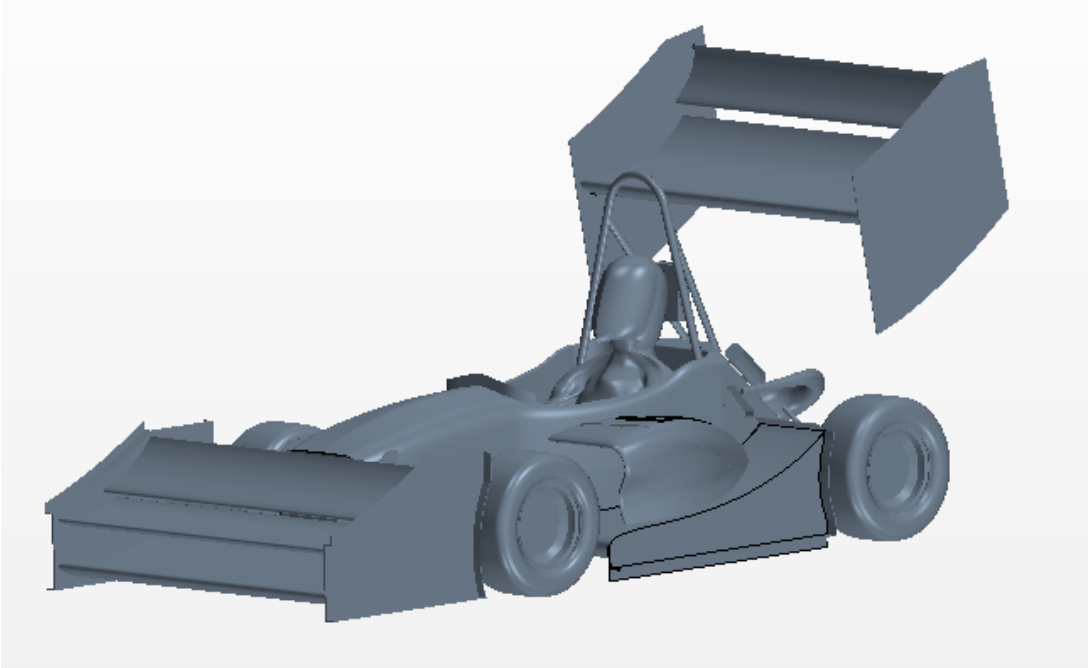

*Figure 56 Full car configuration*

### 4.2.1 Effect on Front Wing

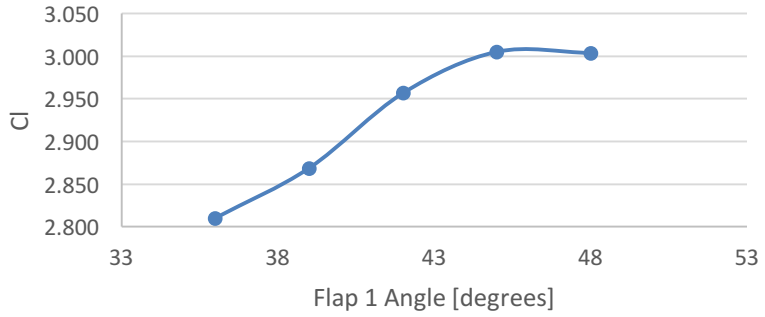


*Figure 57 Front wing Cl vs front wing flap angle*

Figure 57 shows, consistent with literature, that when flap 1 is not stalled, increasing front wing flap angle results in an increase in front wing Cl. The increase is fairly linear between 36 degrees to 42 degrees. Cl is maximum at 45 degrees, then slightly less at 48 degrees.

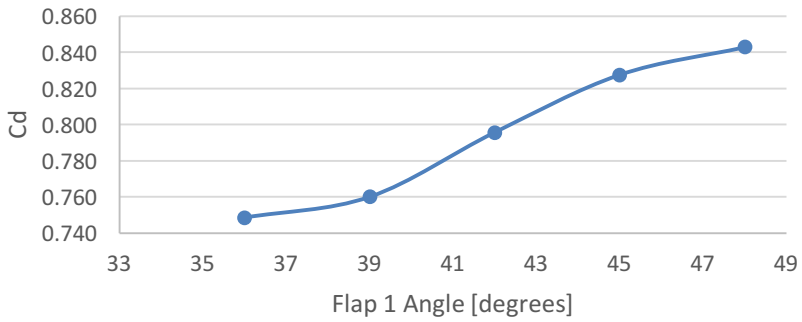


*Figure 58 Front wing Cd vs front wing flap angle*

Figure 58 shows that front wing Cd follows the same increasing trend as front wing Cl, but increases further at 48 degrees.

The velocity distribution in Figure 59 does not show any signs of separation on the elements. The reduction in Cl could be attributed to the interaction between flap 1 and the upper flaps, 2 and 3. Individual downforce reports for each element in Table 14 support this claim.

| **Part** | **45 degrees** | **48 degrees** |
|---|---|---|
| Main element | 100.8 N | 103.0 N |
| Flap 1 | 23.8 N | 24.8 N |
| Flap 2 | 78.6 N | 76.0 N |
| Flap 3 | 20.1 N | 19.4 N |

*Table 14 Downforce comparison by element*

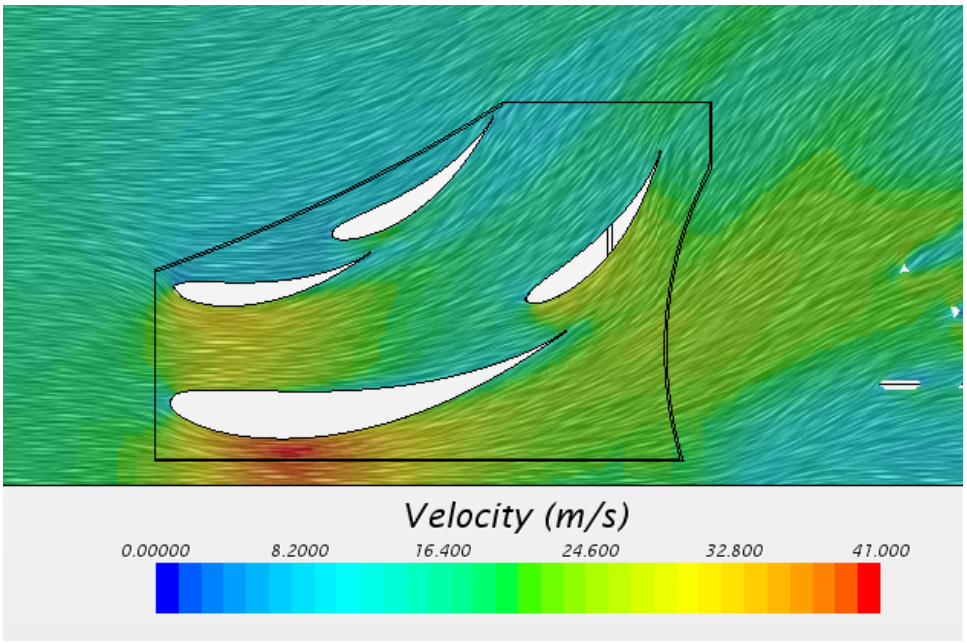


*Figure 59 Velocity distribution on the 0.35m xz plane, front wing flap angle 48 degrees*

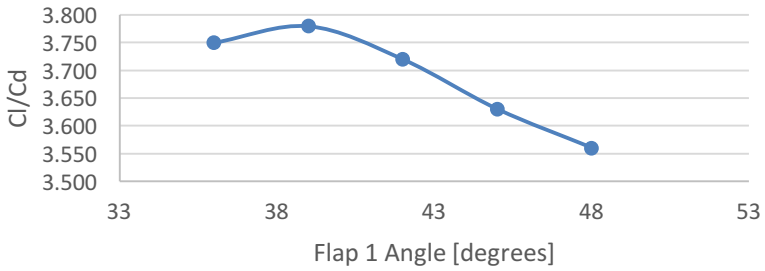


*Figure 60 Front wing Cl/Cd vs front wing flap angle*

Figure 60 shows that the front wing Cl/Cd reaches a maximum value at 39 degrees, decreasing at flap angles above and below.

### 4.2.2 Effect on Rear Wing

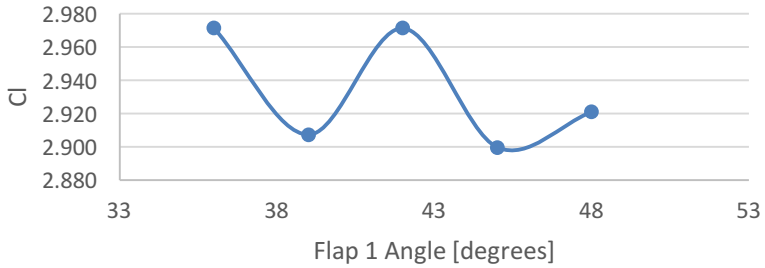


*Figure 61 Rear wing Cl vs front wing flap angle*

Figure 61 shows a general trend of decreasing rear wing Cl with increased front wing flap angle. The change is relatively small, only 2.4% between the minimum and maximum values. Rear wing Cl reduction can be attributed to decrease in incident angle of air at the rear wing caused by the front wing up-wash, shown in Figure 62 and 63, reducing the effective angle of attack. The decrease in rear wing Cl has a lower magnitude than that seen in Section 4.1.2. Again, because the rear wing is downstream of all other aerodynamic components it becomes more difficult to identify trends and obtain consistent results.

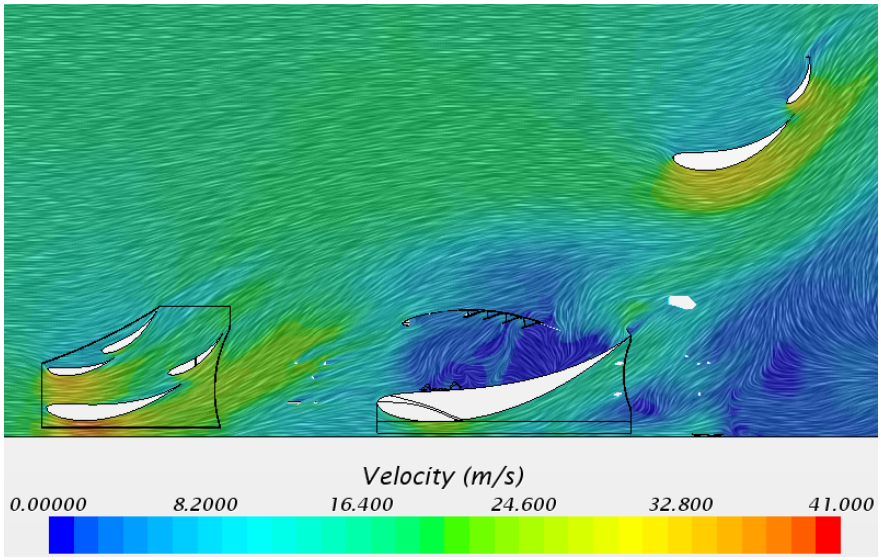


*Figure 62 Velocity distribution on the 0.35 xz plane, front wing flap angle 36 degrees*

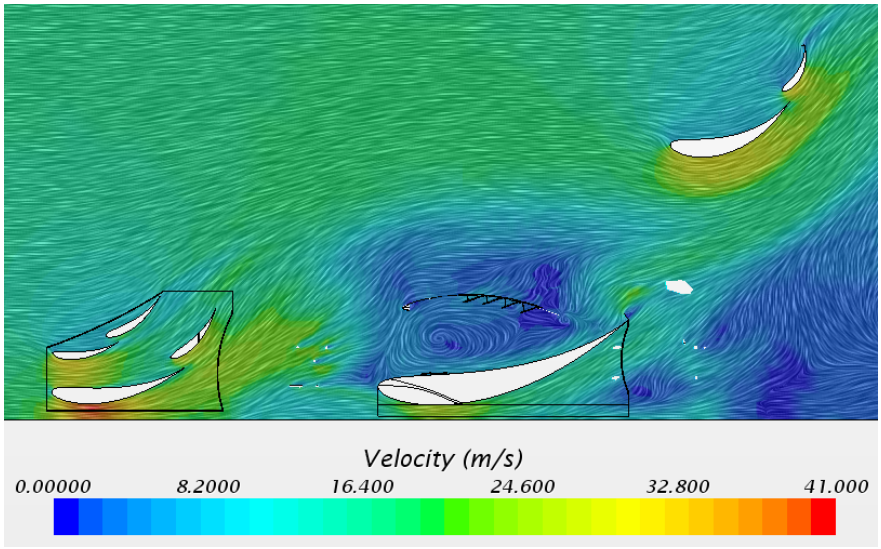


*Figure 63 Velocity distribution on the 0.35 xz plane, front wing flap angle 48 degrees*

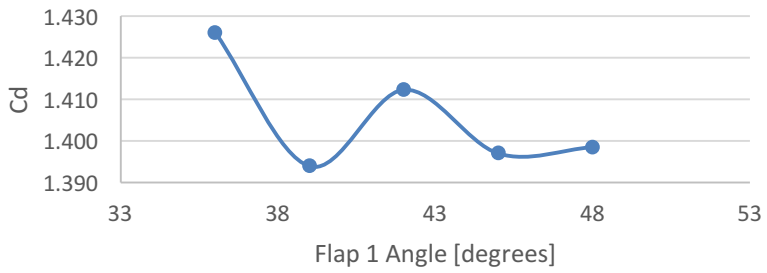


*Figure 64 Rear wing Cd vs front wing flap angle*

Figure 64 shows that the rear wing Cd follows a similar trend to the rear wing Cl curve. As Cl of the rear wing is reduced, so is vortex drag.

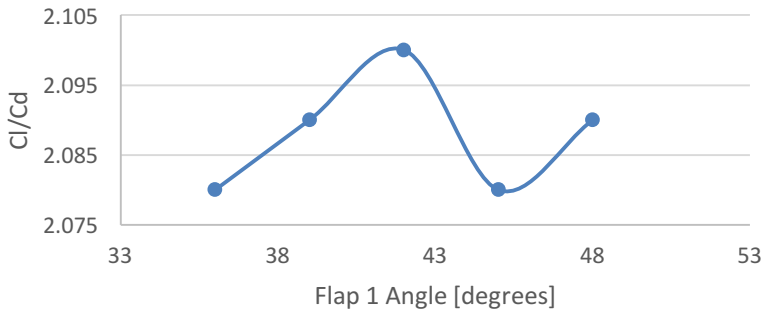


*Figure 65 Rear wing Cl/Cd vs front wing flap angle*

Figure 65 shows that the rear wing Cl/Cd varies slightly, by 1%, as the front wing flap angle is changed. A maximum Cl/Cd value is observed at 42 degrees. Because the changes are so small, a trend cannot be observed.

### 4.2.3 Effect on Undertray

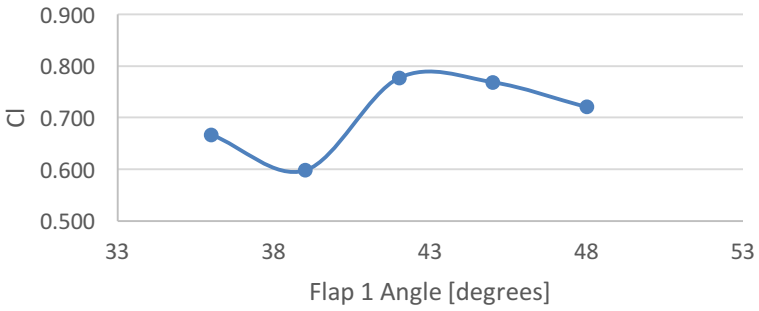


*Figure 66 Undertray Cl vs front wing flap angle*

Figure 66 shows that the maximum Cl of the undertray is reached at 42 degrees and falls above and below. Because the front wing, front tires, undertray, and sidepods are so close together, it would be difficult to determine a Cl relationship without simulation or testing. In this particular configuration 42 degrees provides the highest Cl.

Figure 67 and 68 compare the velocity distributions between the 39 degrees and 48 degrees configurations. It is clear that flow off the front wing in the 39 degrees configuration directs air to and through the sidepod while in the 48 degrees configuration less air is directed to and through the sidepod resulting in an area of recirculation within the sidepod. Consequently, the stagnant air in the sidepod forces more of the air down through the entry of the undertray resulting in an increase in undertray Cl. Pressure distributions, shown in Figure 69 and 70, confirm lower pressure on the bottom of the undertray in the 48 degrees configuration.

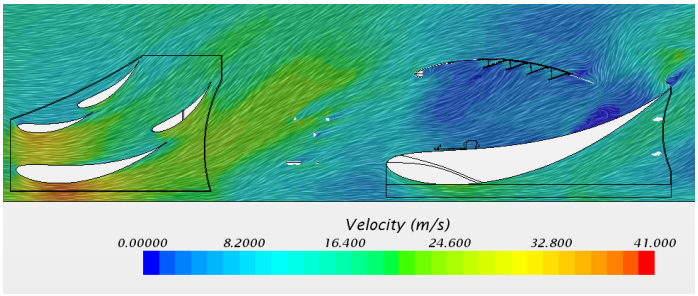


*Figure 67 Velocity distribution on the 0.35 xz plane, front wing flap angle 39 degrees*

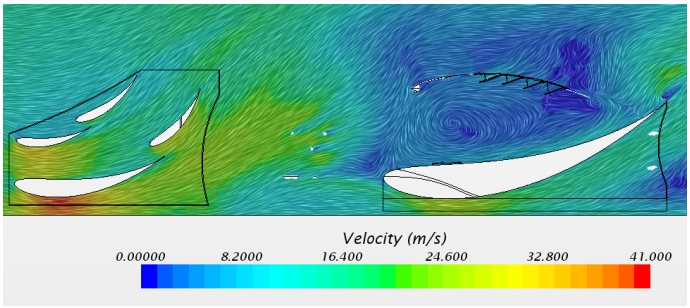


*Figure 68 Velocity distribution on the 0.35 xz plane, front wing flap angle 48 degrees*

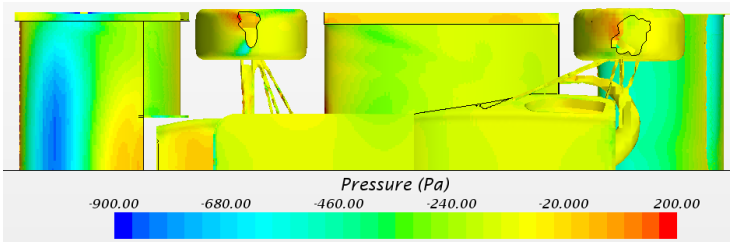


*Figure 69 Pressure distribution, front wing flap angle 39 degrees*

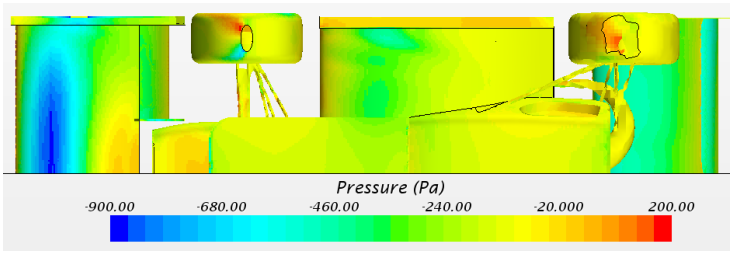


*Figure 70 Pressure distribution, front wing flap angle 48 degrees*

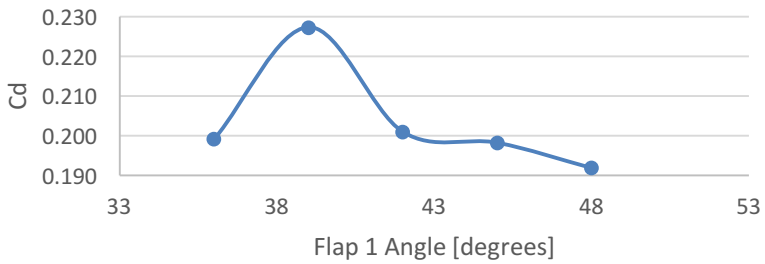


*Figure 71 Undertray Cd vs front wing flap angle*

Figure 71 shows that the maximum undertray Cd occurs at 39 degrees, which also happens to be the lowest undertray Cl. At this flap angle the flow off the front wing appears to be causing some blockage or separation on the undertray.

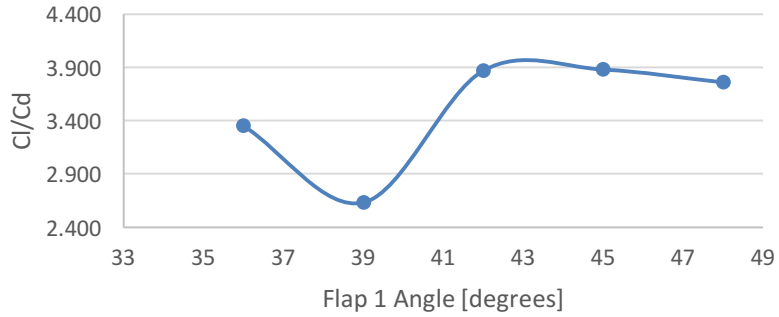


*Figure 72 Undertray Cl/Cd vs front wing flap angle*

Figure 72 shows that the undertray Cl/Cd follows close to the Cl plot. A maximum Cl is reached at 42 degrees and 45 degrees. The change in Cl/Cd is dramatic, varying 47.5% between minimum and maximum values. Designers should pay close attention to this interaction between the front wing flap angle and undertray to choose an appropriate configuration.

### 4.2.4 Effect on Full Car

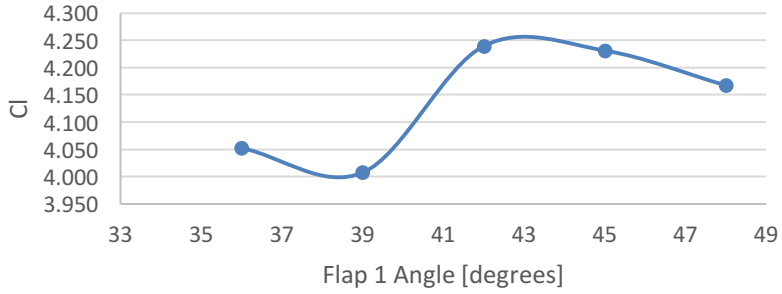


*Figure 73 Full car Cl vs front wing flap angle*

Figure 73 shows that the full car Cl trends up to a maximum at a front wing flap angle of 42 degrees which is the third highest front wing Cl and the highest undertray and rear wing Cl. At this angle the front wing, undertray, and rear wing were working well together to increase full car Cl by 5.7%. This increase in Cl is far less then that observed in Section 4.1.4. This data shows that small front wing flap angle changes can still have a large effect on downstream components.

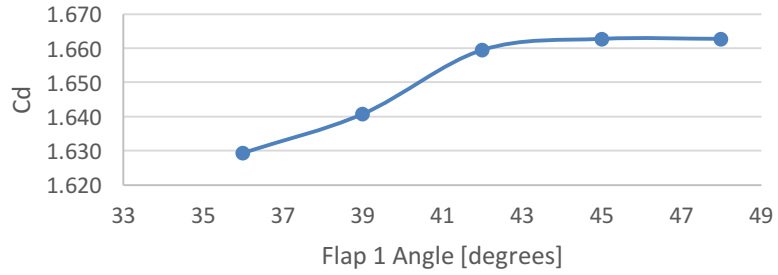


*Figure 74 Full car Cd vs front wing flap angle*

Figure 74 shows that flap angles of 42 degrees, 45 degrees, and 48 degrees all produced similar full car Cd values, within 0.24%. The lowest Cd was observed at the lowest flap angle of 36 degrees with is consistent with isolated wings in ground effect [13] [14].

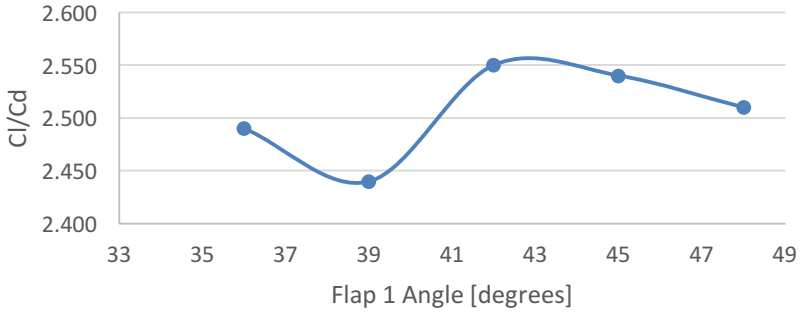


*Figure 75 Full car Cl/Cd vs front wing flap angle*

Figure 75 shows that the full car Cl/Cd is similar to the full car Cl trend, with maximum value at 42 degrees. At this particular angle all aerodynamic components are working well together.

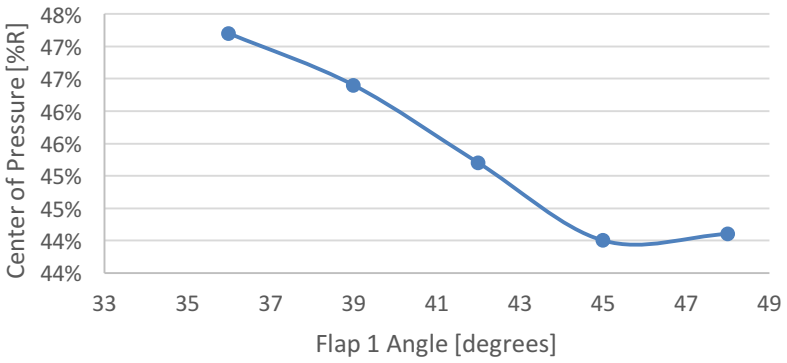


*Figure 76 Center of pressure vs front wing flap angle*

Figure 76 shows that the center of pressure moves forward until 45 degrees as front wing Cl increases and the rear wing Cl and Cd decreases. The slight rearward

movement in center of pressure at 48 degrees can be attributed to the slight decrease in front wing Cl as discussed in Section 4.2.1. The forward movement is only 3.2%, much smaller than the 8% seen in Section 4.1.4. Front wing flap angle changes offer lower potential influences on Cl, Cd, Cl/Cd, and center of pressure than front wing height changes. These changes can be an effective way to make smaller adjustments at the track based on FSAE events or driver preferences.

Table 15 summarizes the general trends of the front wing flap angle of attack study as flap angle is increased.

| **Part** | **Cl** | **Cd** | **Cl/Cd** |
|---|---|---|---|
| Front Wing | Increased | Increased | Decreased |
| Rear wing | Decreased | Decreased | No change |
| Undertray | Increased | Decreased | Increased |
| Full Car | Increased / Decreased | Increased | Increased / Decreased |

*Table 15 Front wing flap angle of attack study summary*

4.3 Rear Wing Angle of Attack and Height Study

In this study, the complete rear wing (including endplates) varies in angle from 0 to 9 degrees and is tested at two heights. The rotation axis is about the leading edge so the main element leading edge height remains constant, mitigating the interferes seen by Wordley and Saunders [7]. The objective of this study is to identify trends in Cl, Cd, Cl/Cd, and center of pressure for different aerodynamic elements and of the complete car.

Figure 77 shows the rear wing used in this study. Figure 78 shows the full car configuration. Table 16 shows the relevant wing geometry.

| **Parameter** | **Value** | **Unit** |
|---|---|---|
| Main Element | | |
| Thickness | 12 | % chord |
| Camber | 10 | % chord |
| Angle of attack | 0-9 | degrees |
| Leading edge height | 1050-1100 | mm |
| Flap 1 | | |
| Thickness | 12 | % chord |
| Camber | 10 | % chord |
| Angle of attack | 26-35 | degrees |
| Flap 2 | | |
| Thickness | 12 | % chord |
| Camber | 10 | % chord |
| Angle of attack | 52-61 | degrees |

*Table 16 Rear wing configuration*

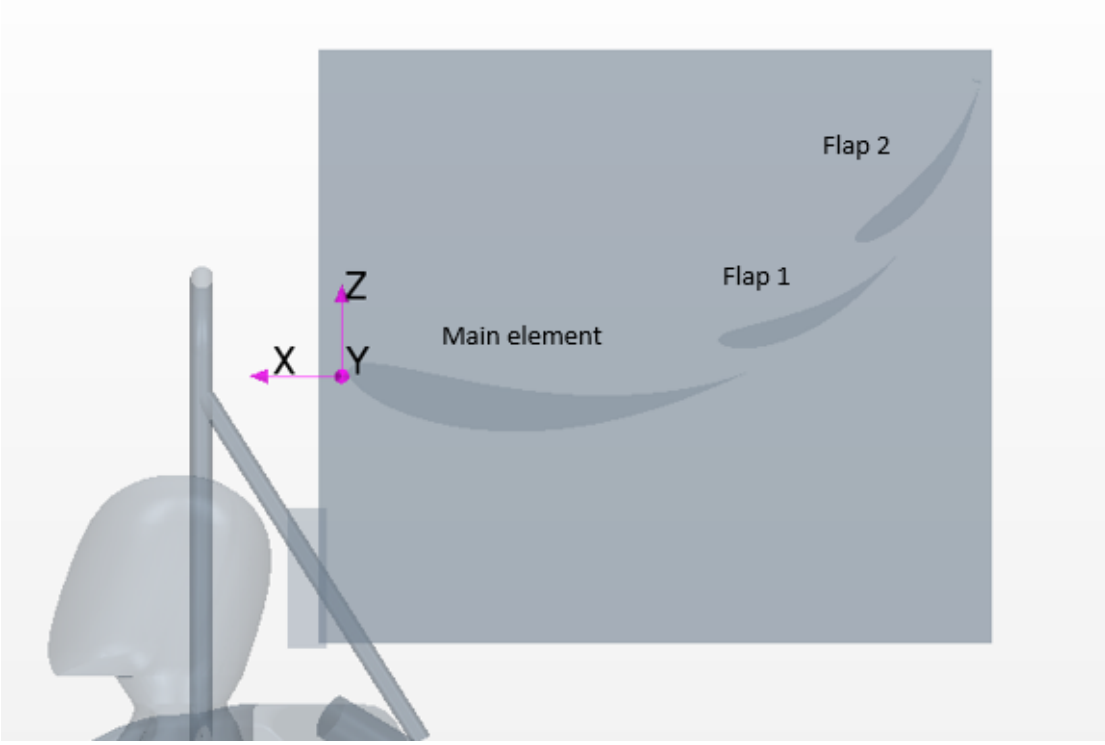


*Figure 77 Rear wing configuration and rotation axis*

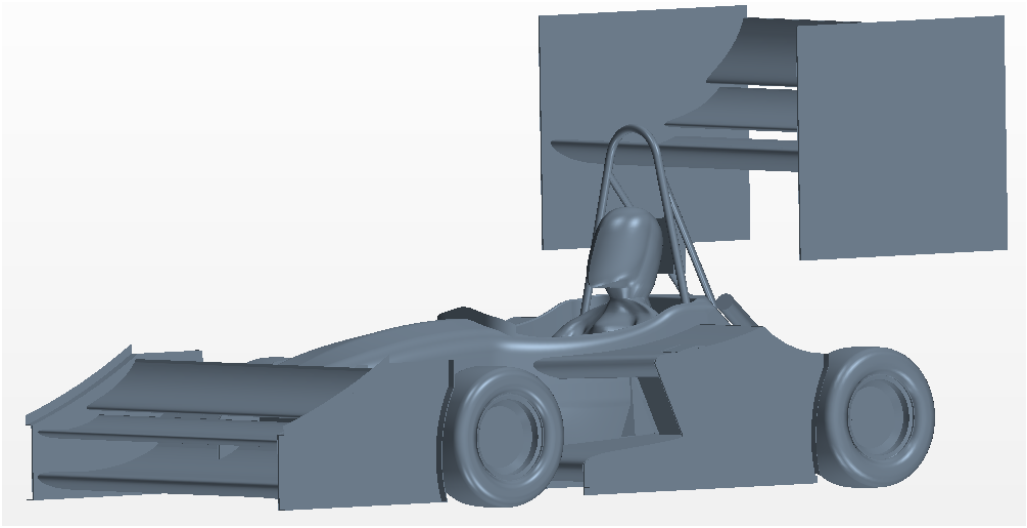

*Figure 78 Full car configuration*

### 4.3.1 Effect on Front Wing

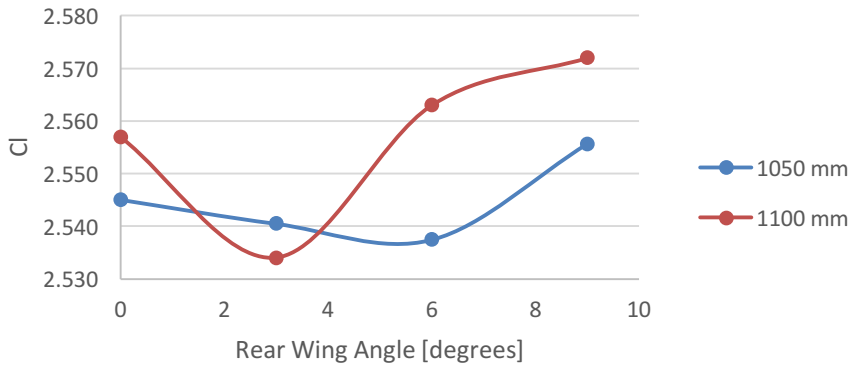


*Figure 79 Front wing Cl vs rear wing angle*

Figure 79 shows the front wing with a slight trend of decreasing Cl until 6 degrees then increasing at 9 degrees in the 1050 mm configuration. The additional height of the rear wing increased front wing Cl at 6 and 9 degrees compared to the 0 degree configuration. The increases were very small, between 1.4% and 2.5%. This data suggests that even though the rear wing is far behind the front wing, its position may have a small effect on front wing Cl.

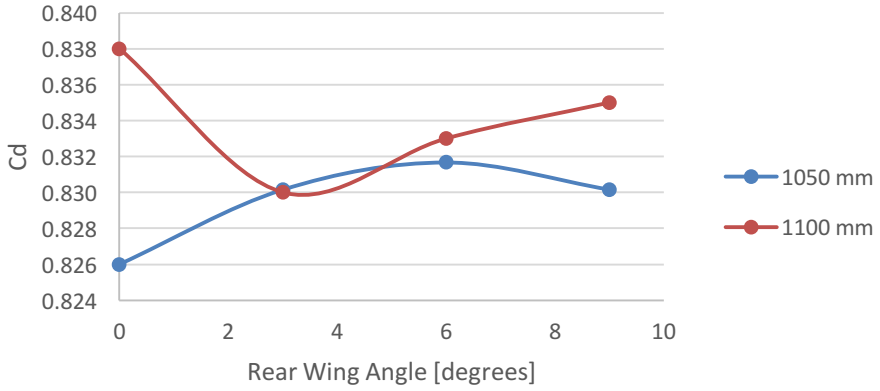


*Figure 80 Front wing Cd vs rear wing angle*

Figure 80 shows a very slight trend of increasing front wing Cd with increasing rear wing angle and height, excluding the 0 degree 1100 mm configuration. The changes in Cd are very small, only 1.5% between all configurations. The increase can be attributed the increased vortex drag accompanied by the higher front wing Cl values.

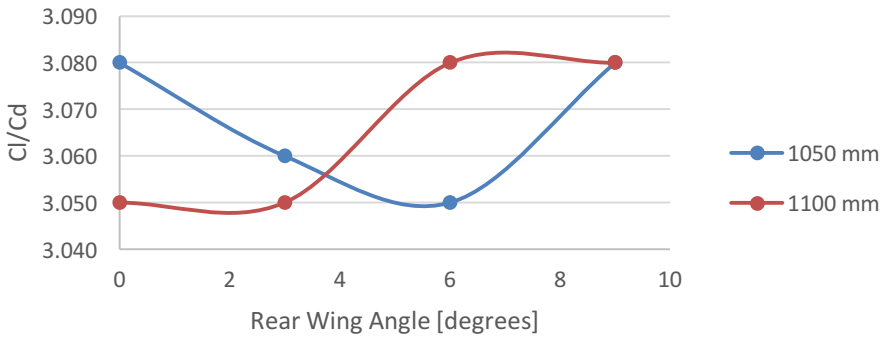


*Figure 81 Front wing Cl/Cd vs rear wing angle*

Figure 81 shows that it is hard to recognize a trend in front wing Cl/Cd with increased rear wing angle or height. Again, the values are only changing slightly, less than 1%. In this case a finer mesh should be used to reduce error.

### 4.3.2 Effect on Rear Wing

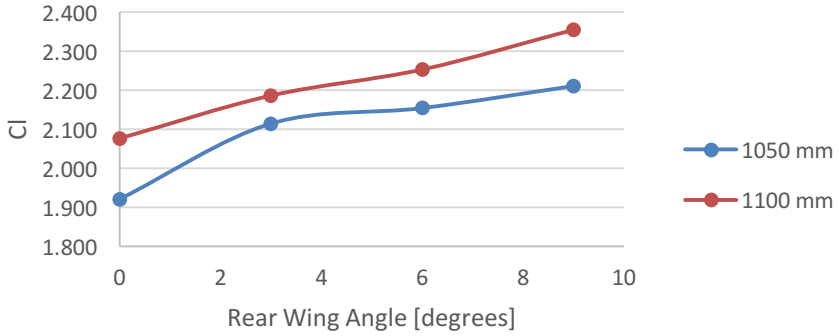


*Figure 82 Rear wing Cl vs rear wing angle*

Figure 82, consistent with [7], shows that the Cl for both rear wing heights, increases, close to linearly, with increased angle of attack. There is no decrease in Cl at 9 degrees, suggesting increased angles could produce higher Cl values. It is evident that the 1100 mm configuration had a higher Cl than the 1050 mm configuration in every position, on average 6% higher.

The results in Sections 4.1.2 and 4.2.2 confirm that front wing h/c and angle is affecting rear wing Cl. Additional rear wing heights should be tested to determine an effective freestream height. These results show a large increase in rear wing Cl, up to 21.6%, is possible without additional weight.

Figure 83 and 84 show the velocity distribution of the 0 degree and 9 degrees, 1050mm height configurations. An increase in air speed on the lower surface of the rear wing is seen in the 9 degrees configuration supporting the increase in Cl for this configuration. No separation is observed in either configuration.

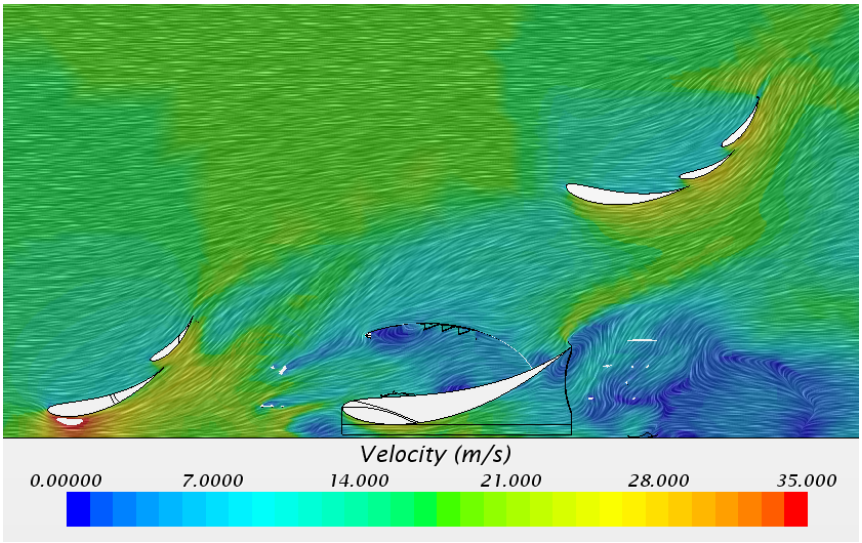


*Figure 83 Velocity distribution on the 0.35 xz plane, rear wing 0 degree and 1050mm*

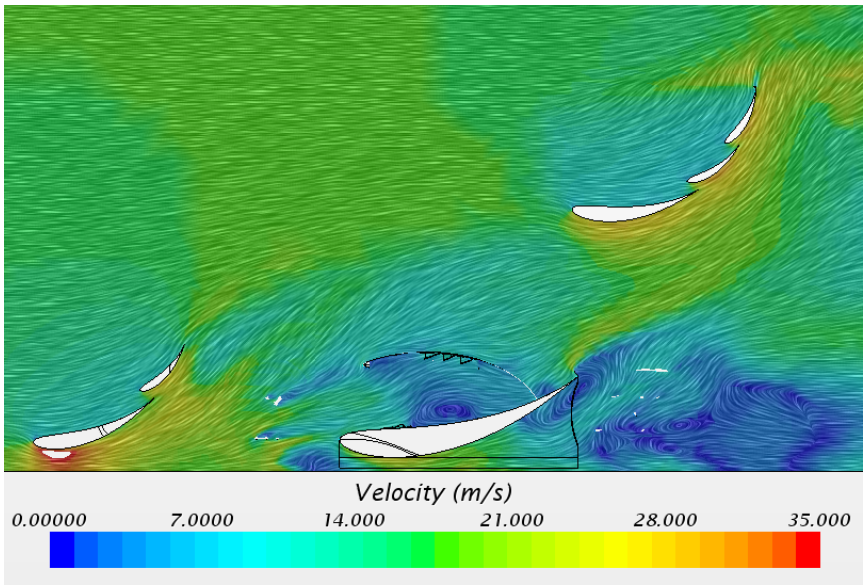


*Figure 84 Velocity distribution on the 0.35 xz plane, rear wing 9 degrees and 1050mm*

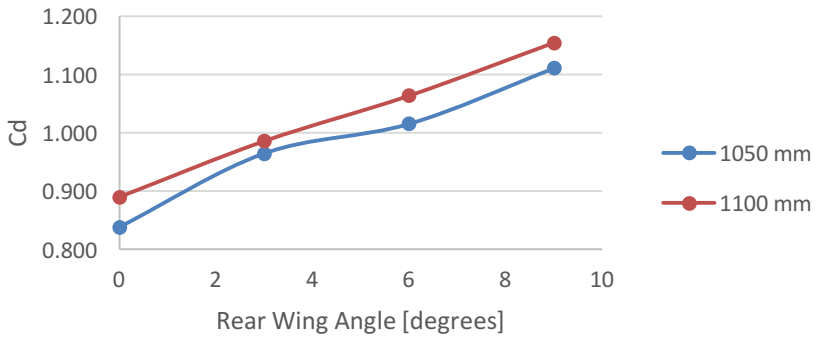


*Figure 85 Rear wing Cd vs rear wing angle*

Figure 85 shows again, consistent with [7], Cd for both heights, increases, close to linearly, with increased angle of attack. The higher rear wing produced higher Cd values in every position, on average 5% higher.

Values of Cd in the 9 degrees 1100 mm configuration are much higher than the 0 degree 1050 mm configuration. Designers should consider how this increased Cd may affect top speed, engine selection, and fuel usage.

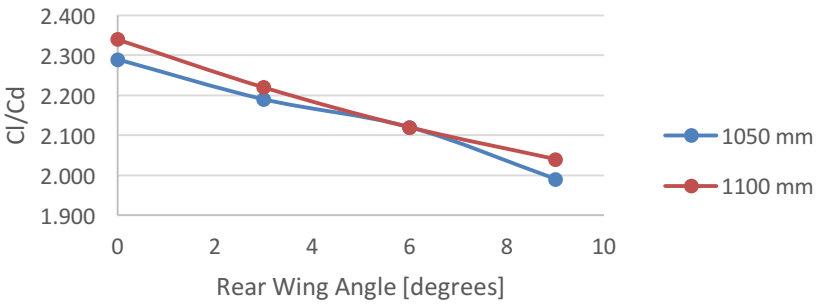


*Figure 86 Rear wing Cl/Cd vs rear wing angle*

Figure 86 shows that the 1100 mm rear wing configuration produces a higher Cl/Cd than the 1050 mm configuration at every angle. This supports Wordley and Saunders [7] that a higher, lower angle of attack wing is more efficient when influenced by other components.

### 4.3.3 Effect on Undertray

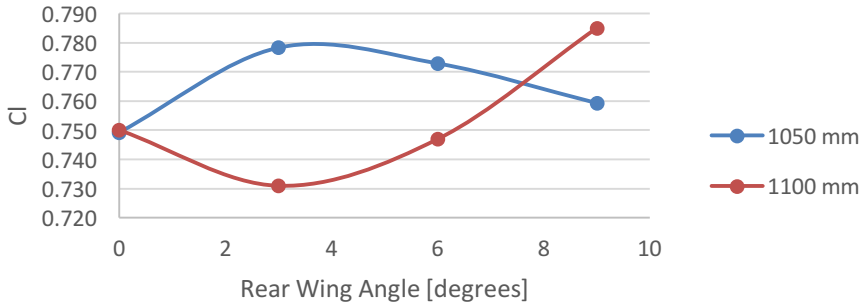


*Figure 87 Undertray Cl vs rear wing angle*

Figure 87 shows a slight trend of increasing undertray Cl with increasing rear wing angle, more prevalent in the 1100 mm configuration. This supports the discussion presented in Section 2.3.2.3. Undertray Cl increases are in the same magnitude as the front wing Cl increases. Figure 88 and 89 show the air flow in the 0 degree and 9 degrees configurations. In the 9 degrees configuration, lower pressure is created beneath the rear wing, above and rearwards of the undertray exit. This low pressure should help to pull air through the undertray, preventing separation. In theory, an undertray with a high angle of attack of could be used by taking advantage of the flow interactions with the rear wing. Different undertray angles should be tested to support this claim.

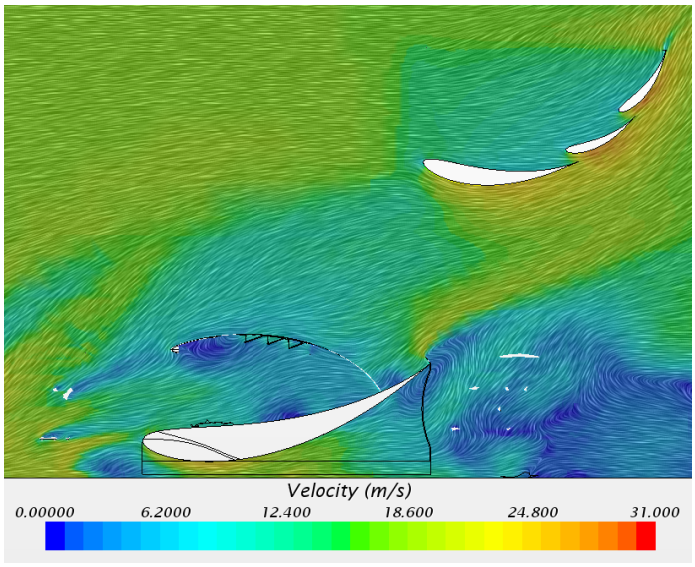


*Figure 88 Velocity distribution on the 0.35 xz plane, rear wing 0 degree and 1050mm*

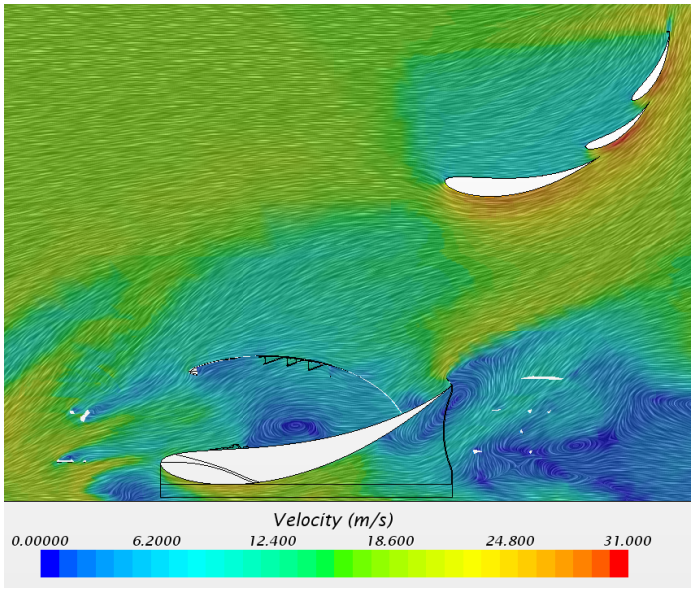


*Figure 89 Velocity distribution on the 0.35 xz plane, rear wing 9 degrees and 1050mm*

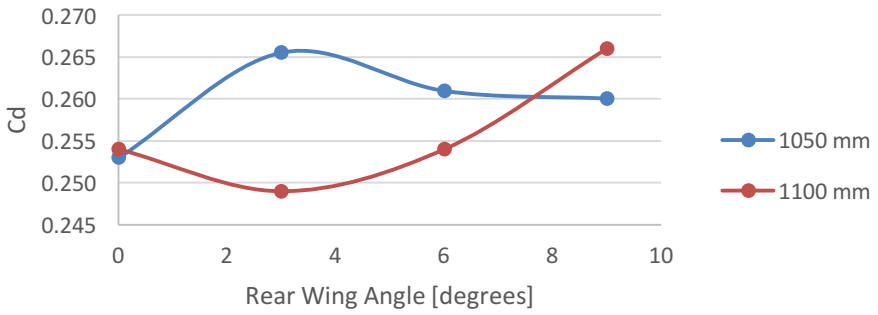


*Figure 90 Undertray Cd vs rear wing angle*

Figure 90 shows that the undertray Cd follows a similar trend to the undertray Cl, increasing slightly at higher rear wing angles of attack. Again, the Cd changes are small, varying by only 6.8% between the minimum and maximum values.

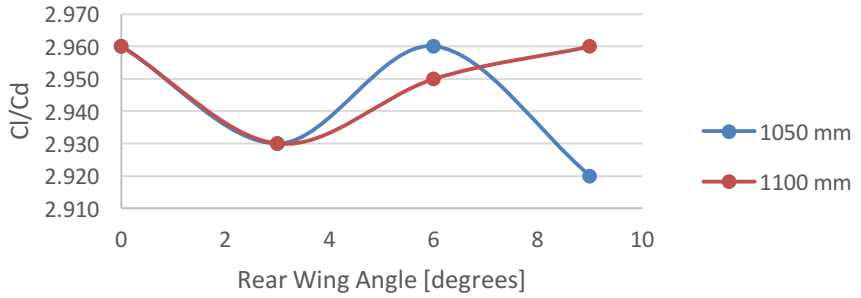


*Figure 91 Undertray Cl/Cd vs rear wing angle*

Figure 91 shows no observable trend in the undertray Cl/Cd at the tested rear wing angles or heights.

### 4.3.4 Effect on Full Car

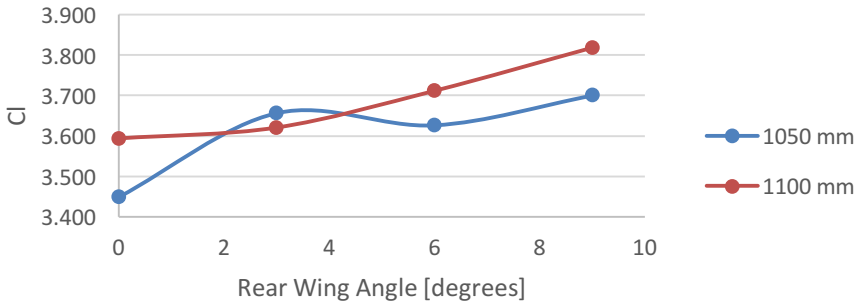


*Figure 92 Full car Cl vs rear wing angle*

Figure 92 shows that the full car Cl increases with increasing angle of attack in all configurations except the 3 degrees 1050 mm configuration. This increase in full car Cl can be attributed to the increase in rear wing Cl at all angles. The additional 50 mm increase in rear wing height increased full car Cl at all angles expect 3 degrees. Although small increases in front wing and undertray Cl were observed, the rear wing angle and height changes have a much more isolated effect on the rear wing alone. This data shows full car Cl can be increased by 10.7% between the minimum and maximum values without additional weight. Even higher Cl values should be possible with increased rear wing angle and height.

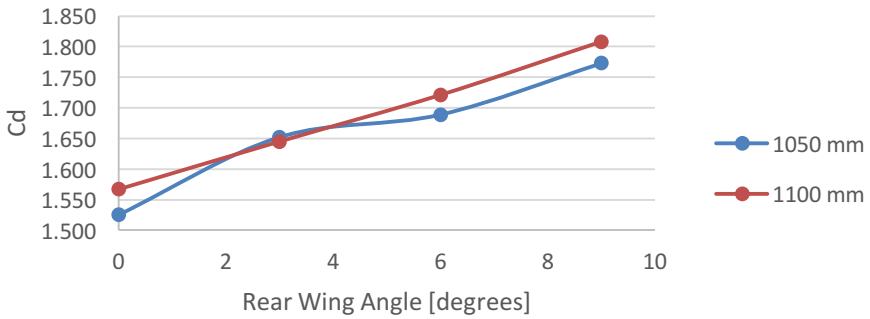


*Figure 93 Full car Cd vs rear wing angle*

Figure 93 shows that the full car Cd follows a similar trend to rear wing Cl increasing as angle of attack is increased. The 1100 mm height increased full car Cd relative to the 1050 mm configuration in all configurations except at the 3 degrees 1050 mm configuration. This increase can be attributed to higher vortex drag as a result of the increase in Cl. As mentioned in Section 4.3.2, designers should consider what impact the higher Cd will have on top speed, engine selection, and fuel usage.

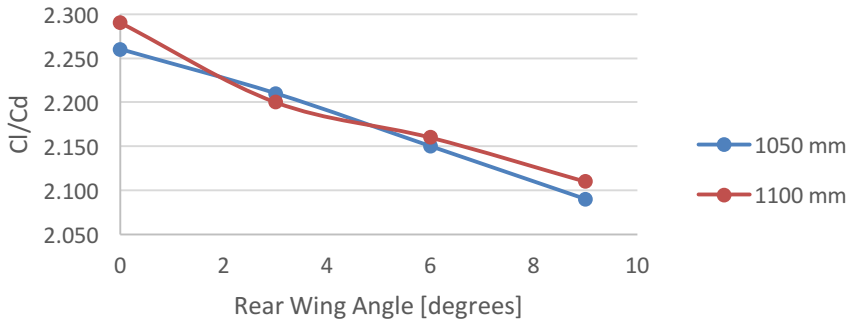


*Figure 94 Full car Cl/Cd vs rear wing angle*

Figure 94 shows that the full car Cl/Cd decreases with increased rear wing angle. Cl/Cd in the 1100 mm configuration was higher than Cl/CD in the 1050 mm configuration except at 3 degrees. As previously discussed in Section 4.3.2 it can be advantageous to use a higher, smaller rear wing to maintain the same Cl/Cd but decrease weight.

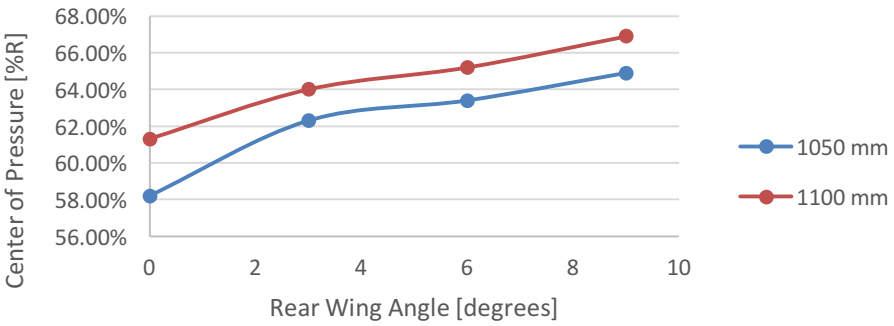


*Figure 95 Center of pressure vs rear wing angle*

Figure 95 shows that the center of pressure moves rearwards with increased rear wing angle and height. This shift is attributed to the higher rear wing Cl and Cd values. The center of pressure change is up to 9% rearwards between the minimum and maximum values. Due to the lower coupled effects on front wing and undertray, overall Cl, Cd, Cl/Cd, and center of pressure can be more easily and consistently be changed by altering rear wing angle and height.

Table 17 summarizes the general trends of the rear wing height study as height is increased.

| **Part** | **Cl** | **Cd** | **Cl/Cd** |
|---|---|---|---|
| Front Wing | Increased | Increased | No change |
| Rear wing | Increased | Increased | Decreased |
| Undertray | Increased | Increased | No change |
| Full Car | Increased | Increased | Decreased |

*Table 17 Rear wing height study summary*

Table 18 summarizes the general trends of the rear wing angle of attack study as angle of attack is increased.

| **Part** | **Cl** | **Cd** | **Cl/Cd** |
|---|---|---|---|
| Front Wing | Increased | Increased | No change |
| Rear wing | Increased | Increased | Decreased |
| Undertray | Increased | Increased | No change |
| Full Car | Increased | Increased | Decreased |

*Table 18 Rear wing angle of attack study summary*

# 5. PHYSICAL TESTING RESULTS

On track physical testing using GFR's 2013 car was conducted to validate aerodynamic performance.

## 5.1 On/Off Test

The purpose of this test was to assess how aerodynamics affected lap times, fuel used, and competition points in the endurance and efficiency events. Two configurations were tested as noted below. The On and Off configurations were chosen to represent an extreme change in Cl and Cd values. Many teams choose not to use and wings at competition. This test will compare the relative performance differences between the two concepts.

**On**: The On configuration, shown in Figure 96, included all wings: front, rear, and undertray. Table 19 shows details of the On configuration.

| Part | Value | Unit |
|---|---|---|
| Front Wing | | |
| Main element | 10 | degrees |
| Flap | 36 | degrees |
| Rear Wing | | |
| Main element | 10 | degrees |
| Flap | 54 | degrees |
| Full Car | | |
| Cl | 3.22 | n/a |
| Cd | 1.43 | n/a |
| Cl/Cd | 2.26 | n/a |
| Center of pressure | 61.7 | % rear |

*Table 19 On configuration*

*Figure 96 On configuration [31]*

**Off**: In the Off configuration the front and rear wings were removed. The undertray remained on the car due to the sidepod position. No ballast was added to compensate for wing weight. Table 20 shows details of the Off configuration.

| Part | Value | Unit |
|---|---|---|
| Full Car | | |
| Cl | -.23 | n/a |
| Cd | .71 | n/a |
| Cl/Cd | -.32 | n/a |
| Center of pressure | -51.8 | % rear |

*Table 20 Off configuration*

*Figure 97 Off configuration [31]*

Raw lap times from the test can be seen in Figure A1. The box plot in Figure 98 shows the lap time differences between the two configurations. The On configuration was, on average, 6.73% faster than the Off configuration. These results are consistent

with the findings from [32]. The variance in lap time for the On configuration was less than the Off configuration representing more consistent lap times and increased drivability of the car. This is particularly important in FSAE autocross and endurance events as explained in Section 1. Statistical analysis shows a P value = 0.0001, which rejects the null hypothesis that the two data sets are the same.

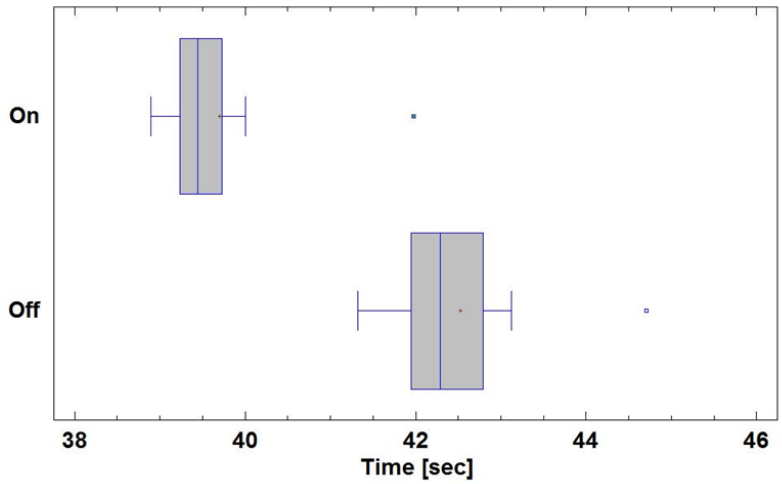


*Figure 98 Box plot of On/Off test lap times*

Figure A2 details the competition scoring results for the endurance and efficiency events based on the lap times and fuel used during the On and Off test. Table 21 summarizes the results. Although more fuel was used in the On configuration, the overall time was lower and more points were earned in the endurance event. Overall the On configuration earns 41.70 more points than the Off configuration in these two events.

| **Event** | **On** | **Off** |
|---|---|---|
| Endurance points /300 | 300 | 245.77 |
| Efficiency points /100 | 87.47 | 100 |
| Total points /400 | 387.47 | 345.77 |

*Table 21 Endurance and efficiency results On/Off*

Logged data comparing a lap between the On and Off configurations, shown in Figure 99 and 100, uncovers details as to why the On configuration was faster. The driver was able to maintain a higher throttle position and higher speed through medium to high speed corners. Brake pressure traces show the driver braking later into the corners and with a higher pressure. Lap time variance shows the Off configuration consistently losing time throughout the entire lap when compared to the On configuration.

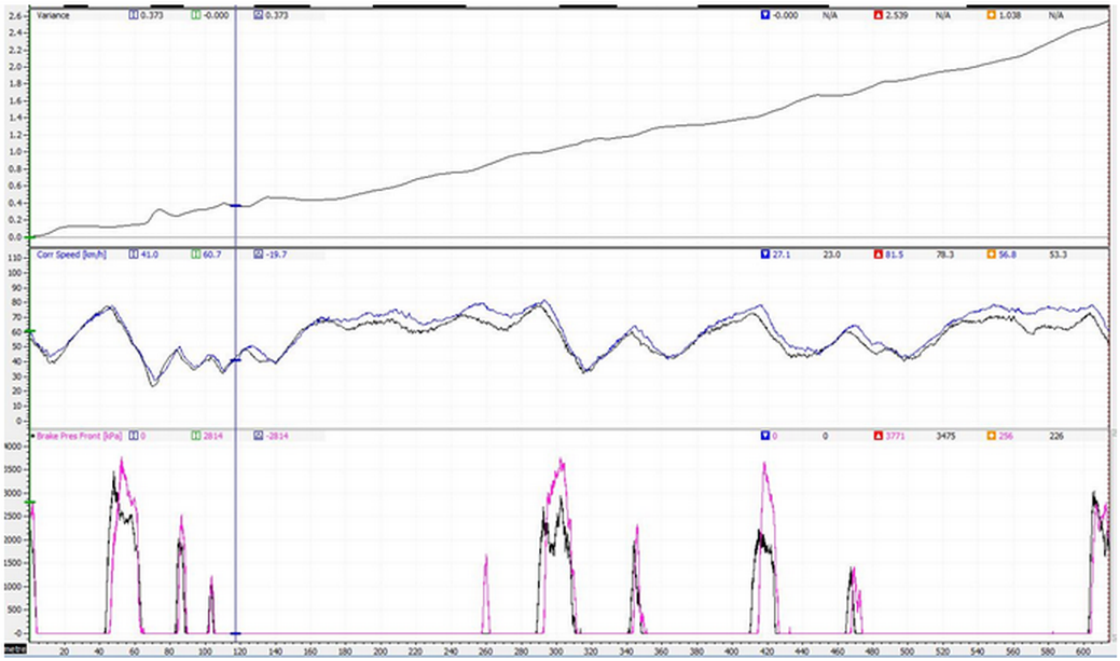


*Figure 99 Logged data from On/Off test, time variance (top), speed (middle), and front brake pressure (bottom). Black traces are Off configuration*

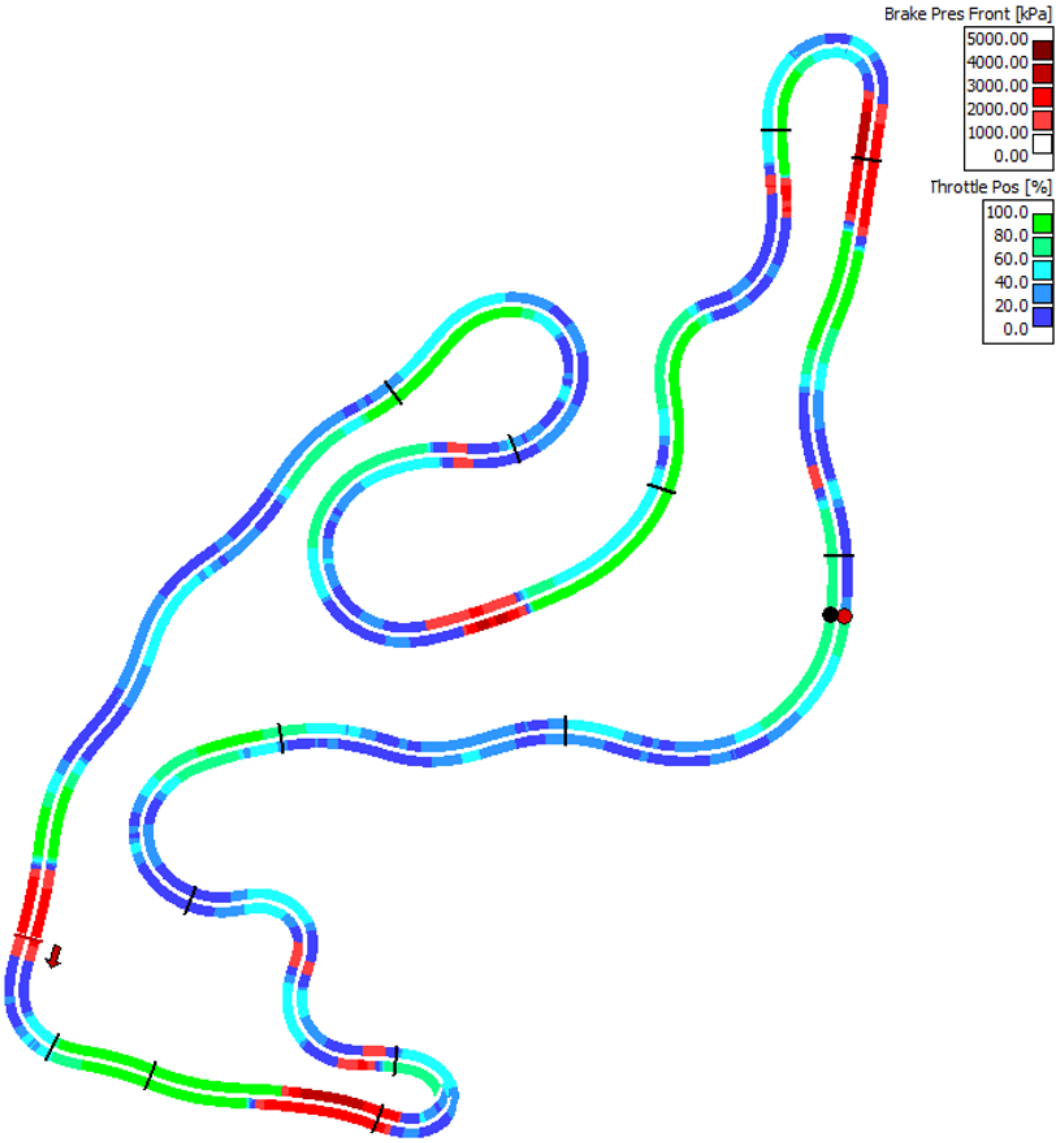


*Figure 100 Track map with throttle position and front brake pressure from On/Off test (inside line is On configuration, outside line is Off configuration)*

5.2 Wing Angle of Attack Test

The purpose of this test was to assess how different wing angles effected on lap times, fuel used, and competition points in the endurance and efficiency events. Two configurations were tested as noted in Table 22 and 23.

**5 degrees:**

| Part | Value | Unit |
|---|---|---|
| Front Wing | | |
| Main element | 5 | degrees |
| Flap | 31 | degrees |
| Rear Wing | | |
| Main element | 5 | degrees |
| Flap | 49 | degrees |
| Full Car | | |
| Cl | 2.91 | n/a |
| Cd | 1.27 | n/a |
| Cl/Cd | 2.28 | n/a |
| Center of pressure | 65.0 | % rear |

*Table 22 5 degrees configuration*

**20 degrees:**

| Part | Value | Unit |
|---|---|---|
| Front Wing | | |
| Main element | 20 | degrees |
| Flap | 46 | degrees |
| Rear Wing | | |
| Main element | 20 | degrees |
| Flap | 64 | degrees |
| Full Car | | |
| Cl | 3.69 | n/a |
| Cd | 1.72 | n/a |
| Cl/Cd | 2.14 | n/a |
| Center of Pressure | 55.0 | % rear |

*Table 23 20 degrees configuration*

Lap times, shown in Figure A3, were 2.39% faster in the 20 degrees configuration compared to 5 degrees configuration. Figure A4 details the competition scoring results for the endurance and efficiency events based on the lap times and fuel used of the 20 degrees and 5 degrees configurations. Table 24 summarizes the results. Although the 20 degrees configuration used 4.38% more fuel, it earned 18.03 more points than the 5 degrees configuration in these two events because the lap times were faster. Statistical analysis shows a P value = 0.004, which rejects the null hypothesis that the two data sets are the same.

| Event | 20 degrees | 5 degrees |
|---|---|---|
| Endurance points /300 | 300 | 280.72 |
| Efficiency points /100 | 98.75 | 100 |
| Total points /400 | 398.75 | 380.72 |

*Table 24 Endurance and efficiency results of wing angle of attack test*

Logged data comparing a lap between the 5 degrees and 20 degrees configurations, shown in Figure 101 and 102, uncovers details as to why the 20 degrees configuration was faster. Similar to the data from the On/Off test, the driver was able maintain a higher throttle position and higher speed through medium to high speed corners. Brake pressure traces show the driver braking later into the corners and but with a similar pressure. The minimum speed was higher by 2.2 kph in the 20 degrees configuration.

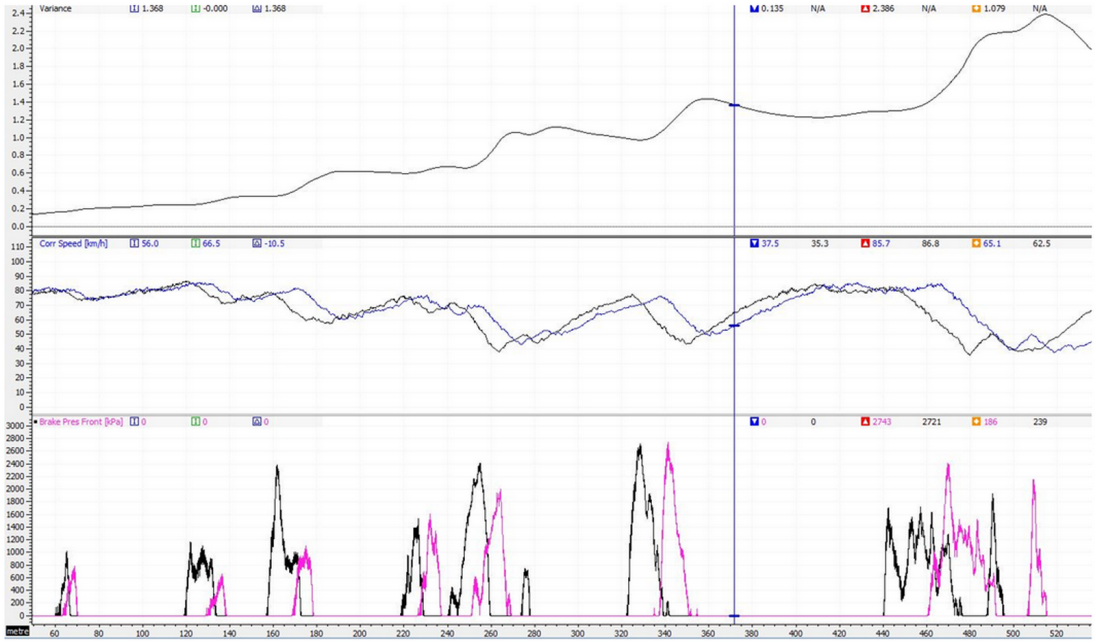


*Figure 101 Logged data from angle of attack test, variance (top), speed (middle), and front brake pressure (bottom). Black traces are 5 degrees configuration*

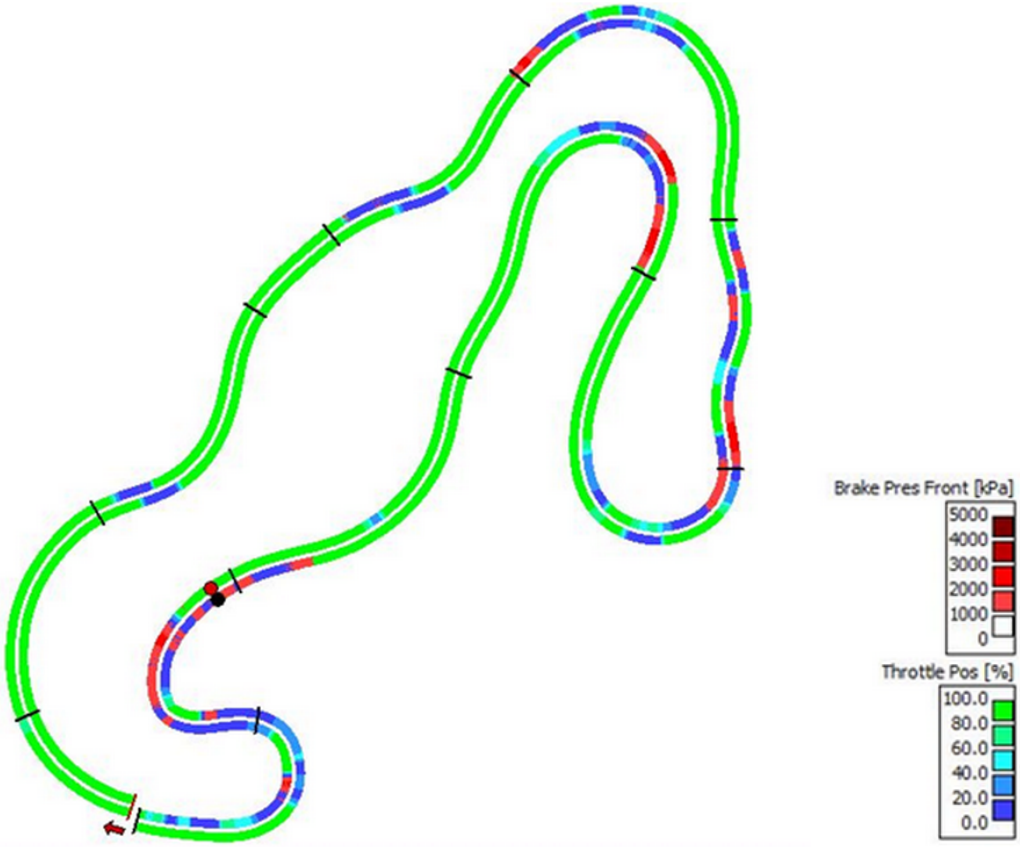


*Figure 102 Track map with throttle position and front brake pressure from angle of attack test (inside line is 20 degrees configuration, outside line is 5 degrees configuration)*

# 6. LIMITATIONS

As discussed in Section 3, there are limitations and unknowns with the CFD model accuracy. Without extensive physical testing the true model error cannot be determined. Based on mesh convergence, a model with reasonable computing time and accuracy was chosen for the simulations. Many simulations correlated with published research for isolated aerodynamic components which supported model validity. The number of simulations conducted for each study was limited by computing resources and project deadlines. A wider range of positions and angles could identify stronger trends. Additionally, simulations with less error are necessary to observe smaller trends. In this case, car shape and wing geometry are somewhat constrained to this particular design, or Formula SAE, meaning one cannot expect trends presented in the thesis to match exactly with their specific car or wing geometry.

Testing data for only two of five dynamic was collected. This limitation is due to the resources available and reliability of the car. Physical testing for the endurance and efficiency events was chosen because it makes up the largest percentage of the dynamics event score and offers reasonable correlation to the autocross event. Future work could expand on the physical testing aspect of this thesis, testing wing configurations for all five dynamic events.

# 7. CONCLUSION

In this thesis FSAE competition events and rules were analyzed with respect to aerodynamics. A CFD simulation model was built and used to conduct a series of sensitivity studies to find trends and relationships of Cl, Cd, Cl/Cd, and center of pressure of individual aerodynamic components and of the full GFR car. Many of the results matched with existing research for isolated components. New research presented in this thesis shows how the individual components interact with each other and change the overall aerodynamic characteristics of the car. The results show simple ways of increasing full car Cl without additional parts or weight. The results help students design aerodynamics for the multi objective nature of the FSAE competition.

Next, four different aerodynamic configurations were physically tested on GFR's 2013 car. Test results showed decreases in lap times of up to 6.73% with wings in the On configuration. Competition points for the endurance and efficiency events were calculated based on lap times and fuel used for the different aerodynamic configurations. Overall, wings on the car earned 41.70 more points than wings off the car. 18.03 more points were earned with the wings in the 20 degrees configuration than the 5 degrees configuration. Logged data confirms the use of aerodynamics increases speed through the corners, decreases braking distances, and increases drivability of the car.

# 8. References


[1] SAE International, *2014 Formula SAE Rules,* 2013.

[2] K. Jensen, "Aerodynamic undertray design for formula SAE," 2010.

[3] SAE International, "Formula SAE Results and Awards," 2015. [Online]. [Accessed 15 June 2015].

[4] P. Wright, "The influence of aerodynamics on the design of Formula One racing cars," *International Journal of Vehicle Design,* vol. 3, no. 4, pp. 383-397, 1982.

[5] J. Katz, Race Car Aerodynamics, Cambridge : Bentley, 2006.

[6] S. McBeath, Competition Car Aerodynamics, Sparkford: Haynes, 2006.

[7] S. Wordley and J. Saunders , "Aerodynamics for Formula SAE: A Numerical, Wind Tunnel and On-Track Study," *SAE Technical Paper,* 2006.

[8] A. Smith, "High-Lift Aerodynamics," *Journal of Aircraft,* vol. 12, no. 6, pp. 501-530, 1975.

[9] W. Jasinski and M. Selig, "Experimental Study of Open-Wheel Race-Car Front Wings," *SAE International,* 1998.

[10] M. Soso and M. Selig, "An Angle of Attack Correction Scheme for the Design of Low Aspect Ratio Wings With Endplates," *SAE Technical Paper 2002-01-3292,* 2002.

[11] X. Zhang and J. Zerihan, "Turbulent Wake behind a Single Element Wing in Ground Effect," Department of Aeronautics and Astronautics, School of Engineering Sciences, University of Southampton, Southampton.

[12] X. Zhang, W. Toet and J. Zerihan, "Ground Effect Aerodynamics of Race Cars," *Applied Mechanics Reviews,* vol. 59, pp. 33-49, 2006.

[13] X. Zhang and J. Zerihan, "Aerodynamics of a Single Element Wing in Ground Effect," *Journal of Aircraft,* vol. 37, no. 6, pp. 1058-1064, 2000.

[14] X. Zhang and J. Zerihan, "Aerodynamics of a Double-Element Wing in Ground Effect," *AIAA Journal,* vol. 41, no. 6, pp. 1007-1016, 2003.

[15] S. Hoerner and H. Borst, Fluid - Dynamic Lift, Albuquerque: Hoerner, 1985.

[16] J. Zerihan and X. Zhang, "Aerodynamics of Gurney Flaps on a Wing in Ground Effect," *AIAA Journal,* vol. 39, no. 5, pp. 772-780, 2001.

[17] G. Altmann, "An Investigative Study of Gurney Flaps on a NACA 0036 Arifoil," San Luis Obispo, 2011.

[18] J. Katz and L. Dykstra, "Study of an Open-Wheel Racing-Car's Rear-Wing Aerodynamics," *SAE Techincal Paper 890600,* 1989.

[19] J. Axerio, G. Iaccarino, E. Issakhanian and K. Lo, "Computational and Experimental Investigation of the Flow Structure and Vortex Dynamics in the Wake of a Formula 1 Tire," *SAE Technical Paper 2009-01-0775,* 2009.

[20] A. Ogawa, T. Takiguchi, S. Yano, S. Nakamura, S. Mashio and M. Shingai, "Development Methodologies for Formula One Aerodynamics," *Honda R&D Technical Review,* pp. 142-151, 2009.

[21] A. Sprot, J. Minto, D. Sims-Williams and R. Dominy, "Aerodynamic Investigation on the Effect of Varying Through-Hub Flow on a Formula One Front Wheel Assembly," *SAE Int. J. Passeng. Cars – Mech. Syst. 4(1):929-944,* 2011.

[22] A. Sprot, D. Sims-Williams and R. Dominy, "The Aerodynamic Characteristics of a Fully Deformable Formula One Wind Tunnel Tyre," *SAE Int. J. Passeng. Cars - Mech. Syst. 5(2):1026-1041,* 2012.

[23] X. Zhang and J. Zerihan, "Edge Vortices of a Double Element Wing in Ground Effect," *Journal of Aircraft,* vol. 41, no. 5, pp. 1127-1137, 2004.

[24] J. Katz and L. Dykstra, "Effect of Wing/Body Interaction on the Aerodynamics of Two Generic Racing Cars," *SAE Technical Paper 920349,* 1992.

[25] E. Cañada, "Aerodynamic analysis and optimisation of the rear wing of a WRC car," Oxford Brookes University, 2012.

[26] L. Roberts, J. Correia, M. Finnis and K. Knowles, "Aerodynamic characteristics of a wing & flap configuration in ground effect & yaw," *J. Automobile Engineering,* 2015.

[27] A. Gopalarathnam and M. Selig, "Design of high-lift airfoils for low aspect ratio wings with endplates," *AIAA Paper 97-2232,* 1997.

[28] N. Ahmad and E. Abo-Serie, "Mesh Optimization for Ground Vehicle Aerodynamics," *CFD Letters,* vol. 2, no. 1, pp. 54-65, 2010.

[29] CD-adapco, "Best Practices for Vehicle External Aerodyanmics," [Online]. [Accessed September 2013].

[30] G. Doig, T. Barber and A. Neely, "The Influence of Compressibility on the Aerodynamics of an Inverted Wing in Ground Effect," *J. Fluids Eng,* vol. 133, no. 6, 2011.

[31] R. Story, "GFR13c Testing," 2013. [Online]. [Accessed 2 Dec 2014].

[32] S. Wordley, J. Pettigrew and J. Saunders , "Aerodynamics for Formula SAE: On-Track Performance Evaluation," *SAE Technical Paper 2007-01-0897,* 2007.

# Appendix A

| | On | | Off | |
|---|---|---|---|---|
| | Laptime [sec] | | Laptime [sec] | |
| | 41.976 | | 44.708 | |
| | 40.007 | | 43.128 | |
| | 39.448 | | 42.789 | |
| | 39.733 | | 42.202 | |
| | 39.520 | | 42.288 | |
| | 39.360 | | 42.560 | |
| | 39.240 | | 41.947 | |
| | 38.897 | | 41.760 | |
| | 39.146 | | 41.332 | |
| | 39.285 | | | |
| | | Fuel Used per lap [l] | | Fuel Used per lap [l] |
| **Average** | **39.661** | **0.0770** | **42.524** | **0.0611** |
| Scaled totals | 1189.836 | 2.310 | 1275.713 | 1.833 |

| | |
|---|---|
| Delta laptimes On to Off | -6.73% |
| Delta fuel On to Off | 20.63% |

*Figure A1 On/Off test raw data*

*Assumptions:*
*90% of co2min*
*100% of Tmin*
*effmin = 35*

| | On | Off |
|---|---|---|
| Tyour | 1189.84 | 1275.71 |
| Tmin | 1189.84 | 1189.84 |
| Tmax | 1725.26 | 1725.26 |
| **endurance score** | **300.00** | **245.77** |
| | | |
| co2min | 3.81 | 3.81 |
| co2your | 5.34 | 4.24 |
| Tmin | 1189.84 | 1189.84 |
| Tyour | 1189.84 | 1275.71 |
| lapyour | 38.00 | 38.00 |
| laptotalmin | 38.00 | 38.00 |
| laptotalco2min | 38.00 | 38.00 |
| | | |
| eff factor | 71.43 | 83.94 |
| effmin | 35.00 | 35.00 |
| effmax | 83.94 | 83.94 |
| | | |
| **eff score** | **87.47** | **100.00** |
| | | |
| **Total Points** | **387.47** | **345.77** |

*Figure A2 On/Off test, endurance and efficiency points comparison*

| | 20 degrees | | 5 degrees | |
|---|---|---|---|---|
| | Laptime [sec] | | Laptime [sec] | |
| | 31.737 | | 32.149 | |
| | 31.428 | | 32.133 | |
| | 30.657 | | 32.289 | |
| | 30.883 | | 31.696 | |
| | 30.719 | | 32.141 | |
| | 31.168 | | 31.303 | |
| | 31.042 | | 31.385 | |
| | 30.884 | | 31.478 | |
| | 31.138 | | 32.157 | |
| | 30.607 | | 31.556 | |
| | 31.124 | | 31.523 | |
| | 30.946 | | 32.025 | |
| | 30.836 | | 31.792 | |
| | 31.165 | | 31.719 | |
| | 31.507 | | 32.354 | |
| | 31.337 | | | |
| | 31.259 | | | |
| | | Fuel Used per lap [l] | | Fuel Used per lap [l] |
| **Average** | **31.085** | **0.0610** | **31.847** | **0.0585** |
| Scaled totals | 1181.212 | 2.319 | 1210.173 | 2.222 |

| | |
|---|---|
| Delta laptimes 20 to 5 | -2.39% |
| Delta fuel 20 to 5 | 4.38% |

*Figure A3 Angle of attack test raw data*

*Assumptions:*
*90% of co2min*
*100% of Tmin*
*effmin = 35*

| | **20 degrees** | **5 degrees** |
|---|---|---|
| Tyour | 1181.21 | 1210.17 |
| Tmin | 1181.21 | 1181.21 |
| Tmax | 1712.76 | 1712.76 |
| **endurance score** | **300.00** | **280.72** |
| | | |
| co2min | 4.62 | 4.62 |
| co2your | 5.36 | 5.13 |
| Tmin | 1181.21 | 1181.21 |
| Tyour | 1181.21 | 1210.17 |
| lapyour | 38.00 | 38.00 |
| laptotalmin | 38.00 | 38.00 |
| laptotalco2min | 38.00 | 38.00 |
| | | |
| eff factor | 86.22 | 87.85 |
| effmin | 35.00 | 35.00 |
| effmax | 87.85 | 87.85 |
| | | |
| **eff score** | **98.75** | **100.00** |
| | | |
| **Total Points** | **398.75** | **380.72** |

*Figure A4 Angle of attack test, endurance and efficiency points comparison*